Cellular/Molecular

Nerve Injury-Induced Neuronal PAP-I Maintains Neuropathic Pain by Activating Spinal Microglia

Jiayin Li,[1]* Haixiang Shi,[2,4]* Hui Liu,[1] Fei Dong,[1,6] Zhiping Liu,[3] Yingjin Lu,[1,5,6] Luonan Chen,[3,4,5] Lan Bao,[2,4] and Xu Zhang[1,4,5,6]

[1]Institute of Neuroscience and State Key Laboratory of Neuroscience, CAS Center for Excellence in Brain Science and Intelligence Technology, University of Chinese Academy of Sciences, Chinese Academy of Sciences, Shanghai 200031, China, [2]State Key Laboratory of Cell Biology, CAS Center for Excellence in Molecular Cell Biology, [3]CAS Key Laboratory of Systems Biology, Institute of Biochemistry and Cell Biology, University of Chinese Academy of Sciences, Chinese Academy of Sciences, Shanghai 200031, China, [4]School of Life Science and Technology, ShanghaiTech University, Shanghai 201210, China, [5]Shanghai Research Center for Brain Science & Brain-Inspired Intelligence, Institute of Brain-Intelligence Technology, Zhangjiang Laboratory, Shanghai 201210, China, and [6]Shanghai Clinical Research Center, Chinese Academy of Sciences/XuHui Central Hospital, Shanghai 200031, China

Pancreatitis-associated proteins (PAPs) display multiple functions in visceral diseases. Previous studies showed that the expression level of PAP-I was low in the DRG of naive rats but was *de novo* expressed after peripheral nerve injury. However, its role in neuropathic pain remains unknown. We found that PAP-I expression was continuously upregulated in the DRG neurons from rat spared nerve injury models, and transported toward the spinal dorsal horn to act as a proinflammatory factor. Intrathecal delivery of PAP-I enhanced sensory hyperalgesia, whereas PAP-I deficiency by either gene knockout or antibody application alleviated tactile allodynia at the maintenance phase after spared nerve injury. Furthermore, PAP-I functioned by activating the spinal microglia via C-C chemokine receptor Type 2 that participated in neuropathic pain. Inhibition of either microglial activation or C-C chemokine receptor Type 2 abolished the PAP-I-induced hyperalgesia. Thus, PAP-I mediates the neuron-microglial crosstalk after peripheral nerve injury and contributes to the maintenance of neuropathic pain.

Key words: **DRG neuron; microglia; neuron-microglial crosstalk; neuropathic pain; pancreatitis-associated protein I; SNI**

Significance Statement

Neuropathic pain is maladaptive pain condition, and the maintaining mechanism is largely unclear. Here we reveal that, after peripheral nerve injury, PAP-I can be transported to the spinal dorsal horn and is crucial in the progression of neuropathic pain. Importantly, we prove that PAP-I mainly functions through activating the spinal microglia via the CCR2-p38 MAPK pathway. Furthermore, we confirm that the proinflammatory effect of PAP-I is more prominent after the establishment of neuropathic pain, thus indicating that microglia also participate in the maintenance phase of neuropathic pain.

Introduction

Pancreatitis-associated proteins (PAPs) belong to a family of secretory proteins. Previous studies suggested the anti-inflammatory or antibacterial functions of PAPs in visceral diseases, such as pancreatitis and bowel syndrome (Dusetti et al., 1993; Bödeker et al., 1998; Gironella et al., 2005; Mukherjee et al., 2014). Among PAP family members, PAP-I may play a protective role by acting as a chemoattractant for macrophages in the ischemic heart (Lörchner et al., 2015). PAP-I secreted by motor neurons after crushing the sciatic nerve both stimulated a survival pathway of motoneurons and triggered Schwann cell proliferation that contributed to the regeneration of motor fibers (Livesey et al., 1997; Nishimune et al., 2000). The expression of both PAP-I and PAP-II was increased in the DRG neurons in the inflammatory pain model (Averill et al., 2008; He et al., 2010; LaCroix-Fralish et al., 2011) and the neuropathic pain models (Averill et al., 2002; Xiao et al., 2002; He et al., 2010; LaCroix-Fralish et al., 2011). Interestingly, PAPs were expressed by small DRG neurons after peripheral in-

Received June 18, 2019; revised Oct. 4, 2019; accepted Oct. 22, 2019.

Author contributions: J.L., L.B., and X.Z. designed research; J.L., H.S., H.L., F.D., and Y.L. performed research; J.L., H.S., and F.D. analyzed data; J.L. wrote the first draft of the paper; J.L., L.B., X.Z., and H.S. revised the paper; Z.L. and L.C. did the computational protein interaction prediction.

This work was supported by the National Natural Science Foundation of China (31630033), the strategic priority research program (B) of Chinese Academy of Sciences (XDPB1005), and the key research program of frontier sciences (QYZDY-SSW-SMC007), Chinese Academy of Sciences, and the Science and Technology Commission of Shanghai Municipality, China (18JC1420301). The funders had no role in study design, data collection and analysis, decision to publish, or preparation of the manuscript.

The authors declare no competing financial interests.

*J.L. and H.S. contributed equally to this work.

Correspondence should be addressed to Xu Zhang at xu.zhang@ion.ac.cn or Lan Bao at baolan@sibcb.ac.cn.

https://doi.org/10.1523/JNEUROSCI.1414-19.2019

flammation induced by complete Freund's adjuvant (CFA), while their expression markedly shifted from small- to large-sized DRG neurons after peripheral nerve injury (Averill et al., 2002, 2008; Costigan et al., 2002; He et al., 2010; LaCroix-Fralish et al., 2011). However, the significance of these expression patterns remains elusive.

DRG neurons are pseudounipolar neurons that the efferent fibers are able to detect noxious stimuli and transfer the nociceptive signals along afferent fibers into the spinal cord; then local circuits in the spinal cord in turn transfer nociceptive signals into the brain to generate the sense of acute pain (Kuner, 2010). If noxious stimulations induced by nerve injury or inflammation persist for a long period of time, nociceptive circuits exhibit tremendous plasticity, enhancing pain signals, producing hypersensitivity, and developing into chronic pain. So far, studies have revealed that the mechanism of chronic pain is complicated and involved changes of neurons and glial cells.

The activation of spinal microglia has been a well-known immune response during the development of neuropathic pain (Chen et al., 2018; Inoue and Tsuda, 2018). After peripheral nerve injury, microglia are quickly activated by sensory neuron-derived proinflammatory factors, such as colony stimulating factor 1 or chemokine (C-C motif) ligand 2 (Thacker et al., 2009; Guan et al., 2016; Okubo et al., 2016), and further aggregate around the central terminals of injured DRG neurons, secreting cytokines and chemokines that can induce the central sensitization (Kettenmann et al., 2011; Tsuda et al., 2013). Several chemokine receptors participate in this process, including C-C chemokine receptor Type 2 (CCR2) and CX3C chemokine receptor 1 (CX3CR1) (Abbadie, 2005; Zhang et al., 2007). Intriguingly, spinal microglia are also known as immune cells in the CNS. Microglia and peripheral macrophage are generated from closely related stem cell lineages and share some gene expression features (Prinz and Priller, 2014). Combining these findings with the report that PAP-I activated peripheral macrophage in the ischemic heart (Lörchner et al., 2015), we postulated that PAP-I secreted by DRG neurons might participate in the immune response during chronic pain.

In the present study, we focused on the function and underlying mechanism of PAP-I after spared nerve injury (SNI), a specific model of neuropathic pain that mimics clinical peripheral nerve injury. The *de novo* expression of PAP-I was also detected in rat DRG neurons after SNI. Nerve ligation in the SNI model showed that a portion of the increased PAP-I transported toward the spinal dorsal horn, unlike the situation in naive condition and peripheral inflammation model, in which PAP-I was only transported to the periphery. SNI-induced PAP-I acted as a central proinflammatory factor required for the maintenance of SNI-induced tactile allodynia via activating microglial CCR2. These findings indicate that PAP-I is an important central signal for peripheral nerve damage, which mediates neuron-microglial interaction in the spinal cord and participates in the maintenance of SNI-induced tactile allodynia.

Materials and Methods

Animals. All experimental procedures were approved by the Committee of Use of Laboratory Animals and Common Facility, Institute of Neuroscience. Animals were kept under a 12 h light/dark cycle at 22°C–26°C. Adult (200–250 g), adolescent (60–80 g), and postnatal day 14 (P14) male Sprague Dawley rats were provided by Shanghai Laboratory Animal Center, Chinese Academy of Sciences (Shanghai, China). The gene knockout (KO) rat was constructed to delete a DNA fragment containing exons 3 and 4 of PAP-I-coding gene *Reg3b* using CRISPR/Cas9 (Biocytogen). The genotyping primers were used as follows: forward 5′-AGA TGTTGCATCGCTTGGCCTTC-3′ for *Reg3b*$^{-/-}$/wildtype (WT); reverse 5′-CAGAAGATCTTGACAAGCTGCCAC-3′ for *Reg3b*$^{-/-}$; reverse 5′-ACTTACTTCTGCATCAAACCAG-3′ for WT.

Animal surgery. SNI and CFA-induced inflammation models were created according to earlier protocols (Decosterd and Woolf, 2000; Liu and Chen, 2012) with minor modifications. Briefly, adult male rats were anesthetized using 2% sodium pentobarbital. For the SNI model, the segments (~0.5 cm) of the common peroneal and tibial nerves in the left thigh (for immunohistochemistry and behavior tests) or both thighs (for immunoblotting and FACS) were exposed and removed, leaving the sural nerve intact. For the CFA-induced inflammation model, a subcutaneous injection of 40 μl CFA was performed at the root of each toe and the center of the left or both hindpaws. The rats were kept in standard environment before further experiments.

Dorsal root ligation and sciatic nerve ligation were performed as previously described (He et al., 2010). After anesthesia, the lumber (L) 4–5 dorsal roots were ligated near the spinal cord ~1.5 cm, and the sciatic nerve was ligated at mid-thigh level with thin and thick suture in rats, respectively. One day after surgery, the rats were killed for further experiments.

Behavior tests. All animals were housed in individually ventilated cages under a 12 h light/dark cycle and given food and water. They were randomly assigned into different groups. All behavior tests were performed double-blinded as previously described (Zhang et al., 2010; Liu et al., 2012b), which complied with the guidelines of the International Association for the Study of Pain. For the rotarod test, the locomotor ability was tested on a rotarod (Xin Ruan, Shanghai, China). The speed was set from 4 to 40 rpm in 5 min, and the running durations before the rats fell off were recorded. For the radiant heat test, rats were put into chambers on flat glass sheets for habituation. After they had maintained a resting state for several minutes, a radiant light was continuously applied to the planar side of their hindpaw until they lifted the hindpaw away. The duration of light application was recorded to represent thermal nociceptive threshold. For the von Frey test, rats were put into chambers on steel mesh for habituation. Then, von Frey filaments were applied to the lateral plantar side of the left hindpaw to measure the mechanical threshold. Each filament was applied at most 5 times, switched to the next filament of either smaller force (if positive response occurred 3 times) or bigger force (if negative response occurred 3 times). The value of the smallest positive force was defined as the mechanical threshold. For the formalin test, formalin (1% in 1 × PBS, 50 μl) was injected subcutaneously into the dorsal part of the left hindpaw, and the nociceptive responses of rats were video-recorded for 1 h. The number of hindpaw flinches in each 5 min interval were counted. For drug treatment, vehicle, PAP-I-Myc-His, or other solutions were intrathecally injected 30 min before formalin injection.

Immunohistochemistry/immunocytochemistry. Adult male rats were fixed with 4% PFA as previously described (He et al., 2010). Cryostat sections of sciatic nerves, L4–5 DRGs, dorsal roots, and spinal cord segments were stained overnight at 4°C with primary antibodies used previously (He et al., 2010) that against PAP-I (1:400, MAB1996, R&D Systems), peripherin (1:1000, AB1530, Millipore Bioscience Research Reagents), S100 calcium binding protein B (S100β, 1:1000, Z0311, Dako), calcitonin-related polypeptide α (1:1000, 24112, Dia Sorin), protein kinase C gamma (1:1000, sc-166451, Santa Cruz Biotechnology), Neurofilament 200 (1:1000, N2912, Millipore Sigma), P2X3 (1:1000, AB5896, Millipore Bioscience Research Reagents), and Iba1 (1:1000, ab5076, Abcam), followed by 40 min incubation at 37°C with secondary antibodies conjugated with FITC, Cy5, and/or Cy3 (1:100, Jackson ImmunoResearch Laboratories). Cultured microglia were fixed with 4% PFA and stained with primary antibody against ED1/CD68 (1:1000, ab31630, Abcam). F-actin was labeled with AlexaFluor-546 phalloidin (1:300, A22283, Invitrogen) for 40 min at 37°C. Fluorescein-conjugated isolectin-I B4 (IB4; 1:1000, FL-1201, Vector Laboratories) was incubated for 40 min at 37°C to label IB4^{+} neurons and fibers. The sections and cells were mounted and scanned using a TCS SP5 or SP8 confocal microscope (Leica Microsystems).

For quantitative analysis of cell number and colocalizing percentage, 3 or 4 sections from each rat and 3 or 4 rats were collected for each group. For quantitative analysis of microglial cell area, 20–30 cells from each experiment and 60–100 cells from 4 independent experiments were collected for each group. The confocal images were processed by ImageJ software. First, several Iba1$^-$ regions were outlined in the dorsal horn to calculate average background signal intensity. Then, the module "subtract background" was used to make the cells more distinguishable, and a default signal intensity threshold with minor adjustments to improve the precision of the area was set to separate Iba1$^+$ microglia from the background signal. After that, the module "analyze particles" was used to analyze the area and average signal intensity of each microglial cell. The actual average intensity of Iba1$^+$ signal in each cell was obtained by deducting background intensity from average signal intensity. And the total Iba1 signal was obtained by adding up the signal of every individual microglia, which was calculated by multiplying the area and average actual signal intensity. The ratio of Iba1$^+$ area in each dorsal horn was obtained by dividing the area of microglia with the area of dorsal horn. For the quantitative analysis of PAP-I signal at ligation points in dorsal root and sciatic nerve, 4–6 rats each group were analyzed. Similar areas of the nerve segments proximal to DRG were selected for analysis. The procedure was similar to the analysis of microglia cell area. The module "analyze particles" was used to calculate the total area of PAP-I$^+$ fibers.

ISH. Adult male rats with or without SNI surgery were perfused with 4% RNase-free PFA as previously described (He et al., 2010). Frozen sections of spinal cord and L4–5 DRGs were fixed and followed by acetylation and prehybridization in the hybridization buffer for 3 h at 67°C, then incubated with the hybridization buffer containing 1 μg/ml of the antisense probe for 16 h at 67°C. Sections were then incubated in alkaline phosphatase-conjugated sheep anti-digoxigenin antibody (1:2000; Roche Molecular Biochemicals). The sections were washed and then developed in a solution of 1 μl/ml NBT and 3.5 μl/ml BCIP in the alkaline phosphatase buffer. The primers for detection of PAP-I mRNA (*Reg3b*) were as follows: 5′-ATGATGAGAGTTAAGATGTTGC-3′ and 5′-TTAA CCTGTAAATTTGCAGACG-3′.

Cell culture, transfection, and protein purification. HEK293 cells were maintained in DMEM (Thermo Fisher Scientific) supplemented with 10% FBS and antibiotics. The coding region of *Reg3b* was cloned from rat DRG cDNA and inserted into the vector pcDNA 3.1/myc-His (−) A. HEK293 cells were transiently transfected with PAP-I-Myc-His using PEI reagent (Millipore Sigma) for 36 h, and then cultured in serum-free Iscove's Modified Dulbecco's Media (Thermo Fisher Scientific) for 2 d. The Iscove's Modified Dulbecco's Media containing secreted PAP-I-Myc-His was collected for protein purification using Ni NTA purification system (Thermo Fisher Scientific). The buffer of purified PAP-I-Myc-His was changed to 1× PBS using Amicon Ultra-4 10K centrifugal filters (Merck Millipore). The protein solution was then diluted to 1 mg/ml and stored under −70°C for later use. To denature PAP-I-Myc-His, the protein was boiled at 100°C for 10 min.

COS7 cells were maintained in DMEM supplemented with 10% FBS and antibiotics. The transient transfection was accomplished using Lipofectamine 2000 reagent (Thermo Fisher Scientific) and 1–4 μg plasmids. AR-42J cells were maintained in Ham's F12K medium (Thermo Fisher Scientific) supplemented with 20% FBS and antibiotics. The cells were cultured for 24–48 h for further experiments.

Primary spinal microglia culture and Boyden chamber assay. The protocol used for primary spinal microglia culture was modified from that of several reports (Silva et al., 1998; Kim et al., 2010; Witting and Möller, 2011). P14 male rats were killed, and the spinal cords were dissected, minced, and sieved. The mixed cells were cultured in DMEM (Thermo Fisher Scientific) with 10% FBS (Biochrom) and 10% horse serum (Thermo Fisher Scientific) in poly-D-lysine (Millipore Sigma)-coated flasks for 14–21 d at 37°C, under 5% CO_2. Primary spinal microglia were resuspended by gently shaking the flasks and then harvested for further assays. The primary microglia were cultured at 37°C, under 5% CO_2 in the following processes.

For morphological analysis, primary spinal microglia were cultured in DMEM in poly-D-lysine-coated dish. After 30 min, the culture medium was replaced to remove cell debris and other types of cells. The relatively purified spinal microglia were cultured for 24 h, and then PAP-I-Myc-His or other drugs were added. The cells were cultured for 48 h before immunocytochemistry assay.

Boyden chamber assay was modified from previous reports (Bianchi et al., 2011; Jeon et al., 2012). Briefly, the primary spinal microglia were cultured in Macrophage-SFM (Thermo Fisher Scientific) for at least 48 h and resuspended at a density of 2×10^5 cells/ml. After 200 μl Macrophage-SFM was loaded into the lower well of Boyden chamber (Neuro Probe), a filter membrane with 8 μm pore (Neuro Probe) was placed on the liquid surface. Then, 200 μl Macrophage-SFM containing 4×10^4 cells was filled into the upper well. The cells were cultured for 7 h to migrate through the membrane from the upper surface to the lower side. For drug treatment, PAP-I-Myc-His was added in the lower well while the inhibitors were added into both upper and lower wells. A cotton swab was used to wipe the unmigrated cells on the upper surface of the membrane, and then the membrane was fixed with 4% PFA and stained with hematoxylin. Neurolucida fluorescent microscope (Nikon) was used to acquire the images. The number of migrated microglia was calculated manually using Image-Pro Plus 6.0 software (Media Cybernetics).

FACS. The protocol used for generating microglia single-cell suspension was modified according to earlier report (Hammond et al., 2019). Briefly, the SNI day 7 and sham control rats were killed, and then L4–6 spinal cord was dissected. Next, tissue samples were dissociated using Dounce homogenizer; the cell suspension was filtered by the Falcon tube with cell strainer cap (Corning). The cells were resuspended in DMEM with 20% Percoll (Yeasen Biotech) and spun down for 30 min to collect the pellet using sorting buffer (0.5% BSA, 1 mM EDTA, in 1 × PBS). All samples were resuspended in sorting buffer containing Cd11b antibody (1:20, CBL1512, Millipore) at 4°C for 1 h, followed by 45 min incubation at 4°C with secondary antibody conjugated with Cy3 (1:10, Jackson ImmunoResearch Laboratories). Microglia were sorted using MA900 (Sony Biotechnology) and then centrifuged for 10 min. Sorted microglia were harvested for further quantitative PCR.

RNA extraction and PCR. The method of single-cell PCR was described previously (Li et al., 2016). The single cultured microglia were aspirated into a glass pipette and gently transferred into lysis buffer; then reverse transcription was performed using a SMARTer Ultra Low RNA Kit (Clontech) directly in the cell lysate. The single-cell cDNA was amplified using an Advantage 2 PCR Kit (Clontech), and the molecular expression was detected using following primers: 5′-GCCAGAGCAAGGATTTGC AG-3′ and 5′-GACCAGTTGGCTTCTGGTGT-3′ for *Iba1* (405 bp), and 5′-ATCCTGCCCCCACTCTACTC-3′ and 5′-AGGGCCACAAGTATG CTGAT-3′ for *CCR2* (447 bp).

The total RNA of sorted microglia was extracted using TRIzol reagent (Thermo Fisher Scientific) and then reverse transcribed, followed by amplification. Quantitative PCR was performed using Hieff qPCR SYBR Green Master Mix (Yeasen Biotech). The molecular expression was detected using the following primers: 5′-AGTGTGAAGCAAATTGGAGC TTG-3′ and 5′-AGTGAGCCCAGAATGGGAGT-3′ for *CCR2* (196 bp), and 5′-GGCAAGTTCAACGGCACAG-3′ and 5′-CGCCAGTAGACTCC ACGAC-3′ for *Gapdh* (142 bp).

The spinal cords were homogenized, and the total RNA was extracted using TRIzol reagent. Then, 1 μg RNA was reverse transcribed to cDNA using the superscript III reverse transcriptase (Thermo Fisher Scientific). Semiquantitative PCR was performed using 2 × Taq Plus Master Mix (Vazyme) and Veriti Thermal Cycler (Applied Biosystems). The molecular expression was detected using following primers: 5′-ATCTCTG CAAGACAGCTAAGGA-3′ and 5′-TCTTGACAAGCTGCCACAGA AT-3′ for *Reg3b* (501 bp), and 5′-CCCAGAACATCATCCCTGCAT-3′ and 5′-GCATGTCAGATCCACAACGGA-3′ for *Gapdh* (134 bp). The bands of PCR samples after electrophoresis were captured by Tanon 1600 (Tanon). The bands were quantified using ImageJ 1.47 software.

Prediction of protein–protein interactions based on a machine learning method. A sequence-based machine learning method (Shen et al., 2007; Liu and Chen, 2012) was adopted to predict the interacting membrane proteins with PAP-I and PAP-II. Totally, 16,456 protein–protein interactions in 4382 rat proteins were used for training a random forest classifier. In which, 8228 experimentally validated protein–protein interactions were collected from six databases as positive samples. The same

number of negative samples was generated by randomly pairwise coupling. For each interaction, the primary sequences of two interacting proteins were encoded into a 686-dimension feature vector by transforming the frequency of amino acid conjoint triads. After training and accuracy evaluation, the predictor was used to screen 5200 membrane proteins in rats for identifying the interactors of PAP-I and PAP-II. Among them, 79 and 231 membrane proteins were predicted to be the partners of PAP-I and PAP-II, respectively, and 71 membrane proteins were predicted to interact with both PAP-I and PAP-II.

Coimmunoprecipitation and immunoblotting. Tissue samples or cultured cells were homogenized in RIPA buffer (150 mM NaCl, 30 mM HEPES, 10 mM NaF, 1% Triton X-100, and 0.01% SDS) with protease inhibitors (1 mM PMSF, 10 mg/ml aprotinin, 1 mg/ml pepstatin, and 1 mg/ml leupeptin). The cell supernatants were incubated with Myc antibodies (Millipore Sigma), and the tissue supernatants were incubated with IgG or CCR2 antibodies (Abcam) overnight at 4°C. The immunoprecipitates and 7.5% total lysates were performed for immunoblotting. The samples were denatured and loaded for SDS-PAGE, and then transferred to nitrocellulose membrane. Primary antibody was applied overnight at 4°C, and secondary antibodies were applied for 1 h at room temperature. The specific protein bands were visualized with chemiluminescence. The primary antibodies include that against PAP-I (1:1000, AF1996, R&D Systems), GAPDH (1:400,000, ab8245, Abcam), actin (1:6000, MAB1501, Millipore Bioscience Research Reagents), Myc (1:1000, self-made), HA (1:2000, H9658, Millipore Sigma), CCR2 (1:1000, ab32144, Abcam), p38 (1:1000, 9212, Cell Signaling Technology), phopspho-p38 (P-p38, 1:1000, 9211S, CST), protein kinase B (Akt, 1:1000, 4631S, Abcam), and phopspho-Akt (P-Akt, 1:1000, 4051S, CST). The immunoreactive bands were quantified from 3 independent experiments using ImageJ 1.47 software (National Institutes of Health).

Electrophysiological recording. L4–6 DRGs of Sprague Dawley rats were dissected and digested with 1 mg/ml collagenase, 0.4 mg/ml trypsin, and 0.1 mg/ml DNase in DMEM for 30 min at 37°C. After trituration, freshly dissociated cells were plated onto coverslips at room temperature, and patch-clamp recording was performed within 6 h. Patch pipettes with 3–5 MΩ resistance were filled with solution containing 135 mM K-gluconate, 0.5 mM $CaCl_2$, 2 mM $MgCl_2$, 5 mM KCl, 5 mM EGTA, 5 mM HEPES, and 5 mM D-glucose, adjusted to pH 7.4 with KOH. The extracellular solution contained 150 mM NaCl, 5 mM KCl, 2.5 mM $CaCl_2$, 1 mM $MgCl_2$, and 10 mM HEPES, adjusted to pH 7.4 with NaOH. Whole-cell current-clamp recording was conducted with an AxonPatch-700B amplifier in voltage-clamp mode with a holding potential of −70 mV and then performed after switching to current-clamp mode. Only the cells with stable resting potentials <-40 mV were used. The data were filtered at 5 kHz and digitized at 20 kHz. The recording chamber was continuously perfused with fresh extracellular solution at a flow rate of 2 ml/min. Cells were immersed in vehicle, PAP-I, or high K^+ (40 mM) solution puffed from a drug delivery system for 30 min. The neuronal excitability was evoked by 1000-ms-long suprathreshold pulses from 0 to 500 pA in increments of 50 pA. To minimize the possibility that the response of glial cells to PAP-I during incubation might affect the neuronal excitability, the injecting pipette of the drug delivery system was placed ~1 mm upstream to the recording cell.

Drug treatment. Minocycline (Selleck) was dissolved in PBS, whereas VX-702 (Selleck) and RS 504393 (Millipore Sigma) were dissolved in DMSO (Millipore Sigma). For morphological assay and Boyden chamber assay, primary microglia were incubated with 200 nM VX-702 (0.4% DMSO) or 700 nM RS 504393 (0.7‰ DMSO). For intrathecal injection, 25 μl minocycline (2 μg/μl) mixed with either 2.5 μl PAP-I-Myc-His (1 μg/μl) or same volume of vehicle was administered via lumber puncture. The 2.5 μl RS 504393 (1 μg/μl) mixed with either 2.5 μl PAP-I-Myc-His (1 μg/μl) or same amount of vehicle was further mixed with 22.5 μl PBS and administered via lumber puncture, and the final concentration of DMSO is 9.1%. For intraplantar injection, 5 μl PAP-I-Myc-His (1 μg/μl) or same amount of vehicle was injected subcutaneously in the hindpaw at the site for subsequent von Frey test or radiant heat test.

Experimental design and statistical analysis. Data are presented as mean ± SEM. Sample number (n) values are indicated in the figure legends. Statistical analysis was performed using Prism 4 (GraphPad Software). Two groups of data were compared using two-tailed, paired, or unpaired Student's t tests. For behavioral tests, two different time curves were compared using two-way ANOVA followed by the test of *post hoc* Bonferroni's multiple comparisons.

Results

PAP-I is *de novo* expressed in DRG neurons and transported to the spinal dorsal horn after SNI

Previous studies showed that the mRNA of PAP-I was present in rat DRG after peripheral nerve injury (Costigan et al., 2002; LaCroix-Fralish et al., 2011). We analyzed the protein level of PAP-I in the DRG of rat SNI model. Immunoblotting showed that the level of PAP-I in DRG was increased as soon as 2 d after SNI ($t = 8.175$, df = 2, $p = 0.0146$), reached peak level between day 7 ($t = 179.500$, df = 2, $p < 0.0001$) and day 14 ($t = 4.841$, df = 2, $p = 0.0401$), then went through a gradual decline (Fig. 1*A*; day 28, $t = 4.447$, df = 2, $p = 0.0470$; day 43, $t = 2.058$, df = 2, $p = 0.1758$). Interestingly, immunostaining showed that PAP-I was not expressed by a certain subpopulation of DRG neurons. Under naive condition, PAP-I was only expressed by few small DRG neurons; whereas after SNI, PAP-I expression was upregulated in large neurons at SNI day 14 (Fig. 1*B–D*). However, PAP-I-positive (PAP-I^+) neurons began to shift from large to small DRG neurons at SNI day 43 (Fig. 1*B–D*). Double-immunostaining detected that, under naive condition, PAP-I was expressed in 0.22 ± 0.10% of total DRG neurons that were all peripherin$^+$, indicating them to be small DRG neurons (Fig. 1*B*,*C*). Fourteen days after SNI, 0.49 ± 0.15% of DRG neurons were PAP-I^+/peripherin$^+$, whereas 3.0 ± 0.36% of DRG neurons were PAP-I^+/S100β^+ (Fig. 1*B*,*C*). S100β is a marker for large DRG neurons. Forty-three days after SNI, 2.45 ± 0.59% of DRG neurons were PAP-I^+/peripherin$^+$ small neurons, whereas 1.67 ± 0.22% of DRG neurons were PAP-I^+/S100β^+ large neurons (Fig. 1*B*,*C*). In addition, ISH and semiquantitative PCR result showed that the PAP-I mRNA was almost absent in the spinal dorsal horn after nerve injury, excluding the possibility that PAP-I was expressed by cells in the spinal dorsal horn (Fig. 1*E*,*F*). Thus, peripheral nerve injury triggers the *de novo* expression of PAP-I only in DRG neurons, the sizes of which shift from small to large and back to small ones.

Since PAP-I was a secretory protein that could be transported to the nerve terminals, we examined the distribution of PAP-I in the peripheral and central fibers of DRG neurons. To observe the transport direction of PAP-I clearly, we ligated the dorsal root and the sciatic nerve to detect the accumulation of PAP-I. Immunostaining showed that, 7 d after SNI, PAP-I accumulated at the ligation sites of both the L4–5 dorsal roots ($t = 5.735$, df = 13, $p < 0.0001$) and the sciatic nerves ($t = 7.221$, df = 7, $p = 0.0002$) on the side proximal to DRGs, whereas it was scarcely observable in intact rats (Fig. 2*A*,*B*). We also observed the trafficking direction of PAP-I 2 d after intraplantar injection of CFA, for PAP-I was also reported to be upregulated in DRG neurons in this model (Averill et al., 2008). Interestingly, in the CFA model, PAP-I was abundant in the sciatic nerve ($t = 7.691$, df = 7, $p = 0.0001$), but was scarcely detected in the dorsal root (Fig. 2*A*,*B*). In addition, triple immunostaining showed that the axons containing PAP-I belonged to large DRG neurons expressing neurofilament 200 (NF200) after SNI, whereas in CFA model, the axons belonged to small DRG neurons expressing P2X3 receptors (Fig. 2*C*). Distribution of PAP-I in NF200$^+$ fibers may represent an increased transportation of PAP-I to the deep layers of spinal dorsal horn. However, immunostaining did not detect the PAP-I signals in spinal dorsal horn. PAP-I may be immediately secreted

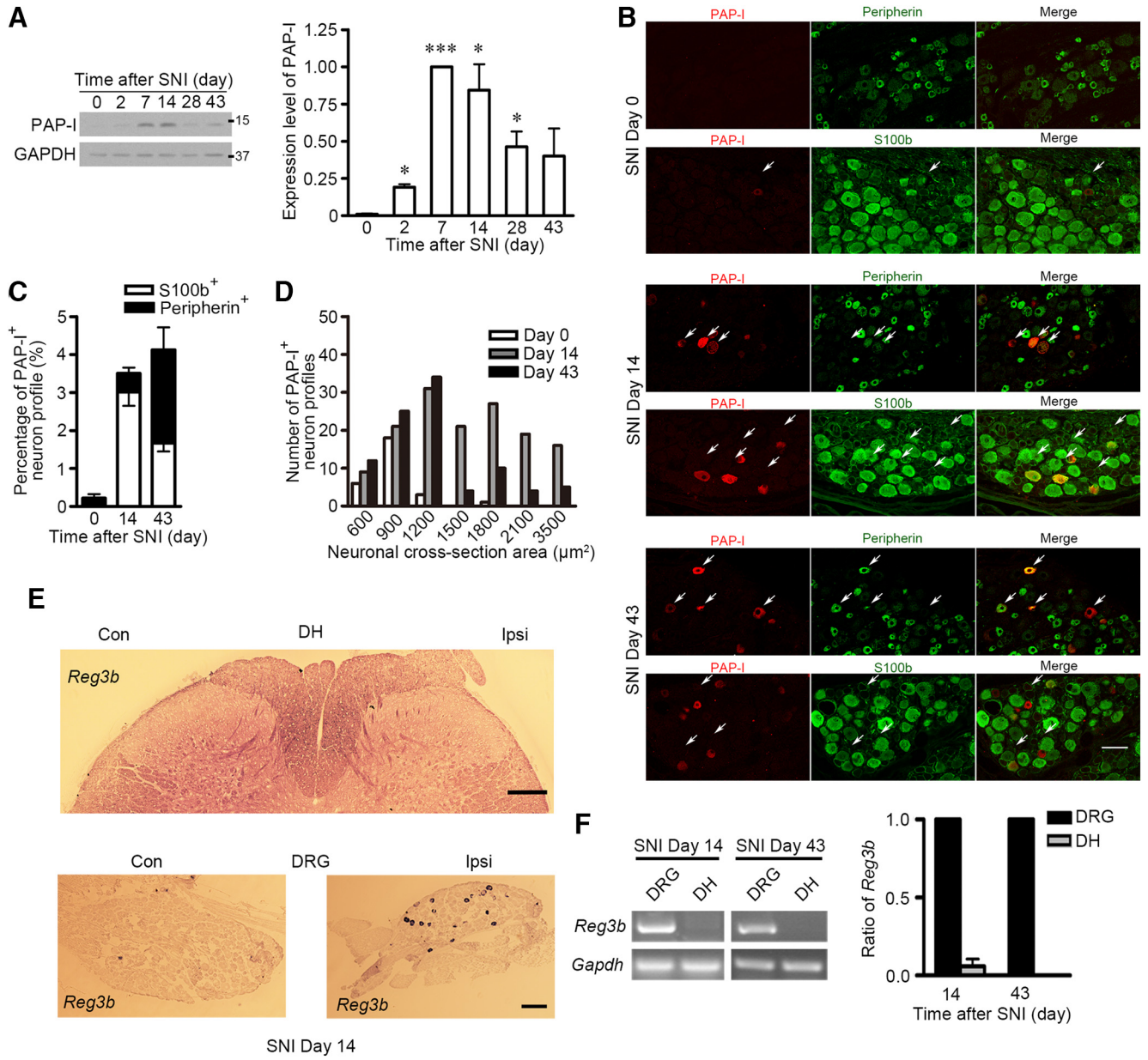

Figure 1. The expression pattern of PAP-I in rat DRG neurons after SNI. ***A***, Immunoblotting showed the upregulation of PAP-I in L4–5 DRGs at different time points (2, 7, 14, 28, 43 d) after SNI (left lane). The quantitative analysis was based on 3 independent experiments. Each sample for immunoblotting was taken from 2 rats. The data were normalized to day 7 (right lane) and shown as mean ± SEM. *$p < 0.05$ versus SNI day 0. ***$p < 0.001$ versus SNI day 0. ***B***, Immunostaining showed that the size of DRG neurons expressing PAP-I (red) after SNI shifted from small (peripherin$^+$, green) to large (S100β^+, green) and back to small ones. White arrows indicate PAP-I$^+$ cells. Scale bar, 100 μm. ***C***, Percentage of PAP-I$^+$ neurons coexpressing peripherin or S100β before and after SNI. Data are mean ± SEM. ***D***, Histogram showing the size changes of DRG neurons expressing PAP-I before ($n = 28$) and after SNI ($n = 143$ for SNI day 14 and $n = 95$ for SNI day 43). ***E***, ISH showed the absence of PAP-I mRNA (*Reg3b*) in ipsilateral (Ipsi) and contralateral (Con) spinal dorsal horn (DH), and the upregulation of DRG neurons, respectively. Scale bar, 200 μm. ***F***, RT-PCR showed that the level of *Reg3b* was almost absent in the spinal dorsal horn compared with that in the DRG at SNI day 14 and day 43. Data were from 3 independent experiments. The data of *Reg3b* were normalized with GAPDH mRNA (*Gapdh*), and then the level in spinal dorsal horn was normalized to that in the DRG. Data are mean ± SEM.

in the nerve terminals of spinal dorsal horn and the amount of PAP-I is relatively low. Together, PAP-I is largely transported via afferent fibers to the spinal dorsal horn only after peripheral nerve injury.

PAP-I in the spinal cord induces hyperalgesia

To examine the function of PAP-I in the spinal dorsal horn, we intrathecally injected the recombinant PAP-I-Myc-His purified from the culture medium of HEK293 cells expressing this protein (Fig. 3*A*) into naive rats. Intrathecal application of 2.5 μg PAP-I-Myc-His per rat induced thermal ($F_{(1,84)} = 5.723$, $p = 0.0190$) and mechanical hyperalgesia ($F_{(1,48)} = 7.197$, $p = 0.0100$; 3 h, $t = 3.514$, df = 8, $p = 0.0079$; 4 h, $t = 3.182$, df = 8, $p = 0.0130$) in naive rats as well as enhanced the Phase II nociceptive behavior ($t = 2.553$, df = 12, $p = 0.0253$) induced by formalin injection ($F_{(1,24)} = 7.893$, $p = 0.0097$) (Fig. 3*B–E*). On the contrary, intrathecal injection of the same amount of denatured PAP-I-Myc-His did not affect nociceptive thresholds and the formalin-induced nociceptive behavior in rats, indicating the specificity of PAP-I-Myc-His effect (Fig. 3*F–I*) (Fig. 3*F*; $F_{(1,60)} = 1.956$, $p = 0.1667$; Fig. 3*G*; $F_{(1,84)} = 1.476$, $p = 0.2277$; Fig. 3*H*; $F_{(1,72)} = 0.157$, $p = 0.6932$; Fig. 3*I*; Phase I, $t = 0.682$, df = 6, $p =$

0.5207; Phase II, $t = 0.141$, df = 6, $p = 0.8929$). Therefore, PAP-I is pronociceptive in the spinal cord.

As PAP-I was also transported to the peripheral tissues, we further studied whether peripherally applied PAP-I-Myc-His could also induce hyperalgesia in naive rats. The behavior results showed that, unlike intrathecal injection, intraplantar injection of 5 μg PAP-I-Myc-His did not cause thermal ($F_{(1,72)} = 0.123$, $p = 0.7269$) or mechanical hyperalgesia ($F_{(1,78)} = 0.989$, $p = 0.3231$) (Fig. 3*J*,*K*). Together, PAP-I has a distinct pronociceptive effect only in the spinal cord but not in the periphery.

PAP-I in the spinal cord participates in the maintenance of neuropathic pain

To verify whether the upregulation of PAP-I plays a role in neuropathic pain, we constructed the PAP-I gene KO rat. A DNA fragment, including exons 3 and 4 of PAP-I-encoding gene *Reg3b*, was deleted (*Reg3b*$^{-/-}$) using CRISPR/Cas9, so that most of the protein-coding sequence was missing (Fig. 4*A*). Immunoblotting combined with immunohistochemistry confirmed that PAP-I was totally absent in the DRG neurons of these rats after peripheral nerve injury (Fig. 4*B*,*C*), suggesting successful KO of PAP-I in rats. Since the augment of PAP-II in injured DRG neurons was reported previously (He et al., 2010), loss of PAP-I staining in KO rats also implied the absence of cross-reaction of PAP-I antibody against PAP-II. Immunoblotting confirmed that PAP-I antibody did not cross-react with PAP-II in HEK293 cells expressing PAP-II-myc-his (Fig. 4*D*), further supporting the excellent specificity of PAP-I antibody.

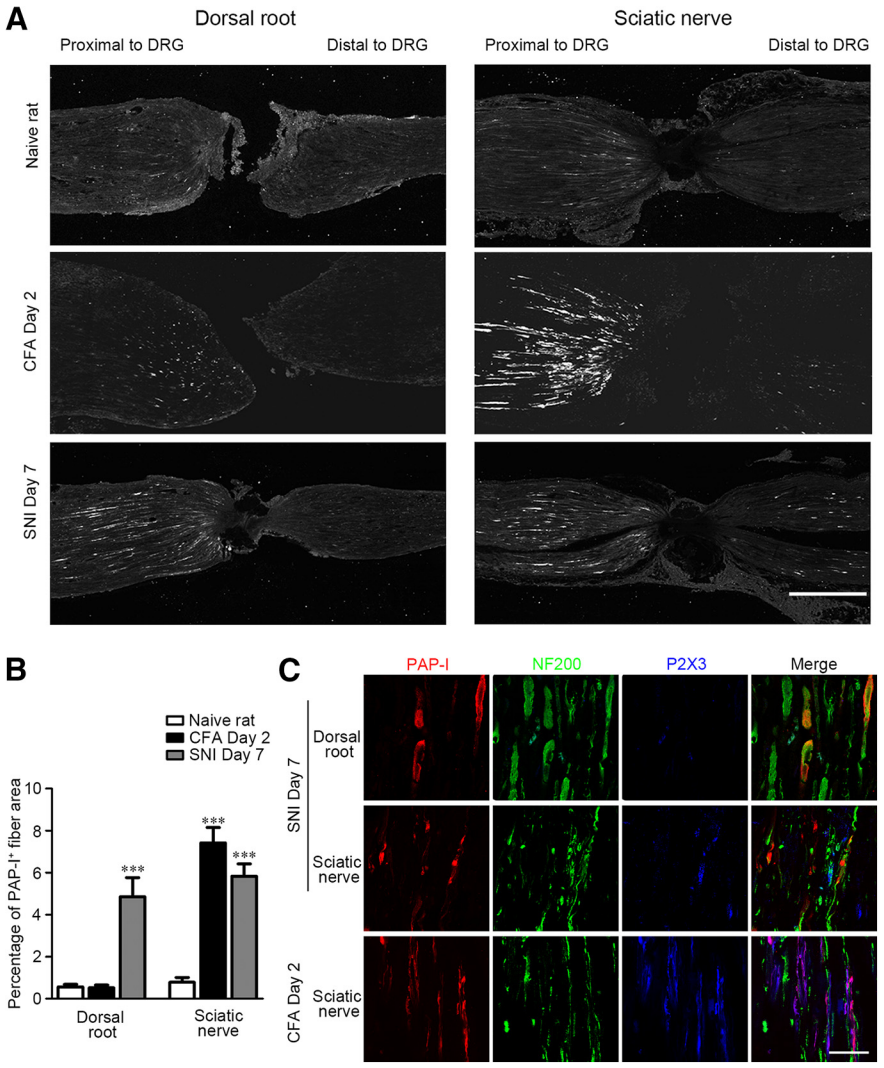

Figure 2. PAP-I is differently transported to the dorsal root and the sciatic nerve in inflammatory and nerve injury models. ***A***, ***B***, Immunostaining after dorsal root (L4–5) and sciatic nerve ligation showed that PAP-I was rarely present along DRG axons in naive rats but was accumulated at the ligation points of the sciatic nerve in CFA day 2 rats and of the dorsal root and sciatic nerve in SNI day 7 rats. Scale bar: ***A***, 500 μm. ***B***, The PAP-I$^+$ fiber area was measured for quantitative analysis ($n \geq 4$). ***$p < 0.001$ versus naive rats. Data are mean ± SEM. ***C***, Immunostaining showed that PAP-I was colocalized with NF200$^+$ fibers (Aβ fibers) in the dorsal root of rats at SNI day 7 and with P2X3$^+$ fibers (C fibers) in the sciatic nerve of rats at CFA day 2. Scale bar, 50 μm.

We first analyzed the behavior of *Reg3b*$^{-/-}$ rats and their WT littermates under normal condition. The body weight of *Reg3b*$^{-/-}$ rats was similar to their littermates ($t = 0.333$, df = 9, $p = 0.7466$); thus, the overall development and metabolism should be normal (Fig. 4*E*). The basal nociceptive thresholds ($t = 0.649$, df = 33, $p = 0.5209$) and motor function ($F_{(1,39)} = 0.008$, $p = 0.9309$) of *Reg3b*$^{-/-}$ rats were also similar with that of their WT littermates (Fig. 4*F*,*G*), indicating that the lack of transient embryonic PAP-I expression in DRG neurons and motor neurons (Nishimune et al., 2000) does not affect neural circuit development.

Next, we analyzed the nociceptive behaviors of *Reg3b*$^{-/-}$ rats under chronic pain condition. After SNI, *Reg3b*$^{-/-}$ rats and their WT littermates both developed tactile allodynia within the first week (Fig. 4*G*). However, as soon as SNI day 14, the tactile allodynia in *Reg3b*$^{-/-}$ rats was alleviated, whereas it was maintained at a severe extent in their WT littermates (Fig. 4*G*). This difference reached statistical significance at day 43 ($F_{(1,189)} = 14.410$, $p = 0.0002$; day 43, $t = 2.762$, df = 24, $p = 0.0108$) (Fig. 4*G*). Furthermore, an intrathecal injection of specific antibody against PAP-I into SNI model rats was applied to examine the effect of acute PAP-I deficiency. In accordance with the behavior results of *Reg3b*$^{-/-}$ rats, blocking PAP-I with the antibody at SNI day 7 had no pain-relieving effect ($F_{(1,60)} = 0.902$, $p = 0.3461$), whereas a very prominent antinociceptive effect was observed at SNI day 28 ($F_{(1,54)} = 11.190$, $p = 0.0015$) (Fig. 4*H*,*I*). The alleviation of mechanical allodynia was most significant at ~2–3.5 h (2 h, $t = 3.999$, df = 9, $p = 0.0031$; 3.5 h, $t = 2.716$, df = 9, $p = 0.0238$) after the antibody injection (Fig. 4*I*). Therefore, the results obtained from both *Reg3b*$^{-/-}$ rats and PAP-I antibody treatment indicate that, after SNI, PAP-I is not necessary in the initiation of tactile allodynia but is a major factor for its long-term maintenance.

Since PAP-I was also upregulated in DRG neurons after peripheral inflammation induced by CFA, the behavioral tests were performed on *Reg3b*$^{-/-}$ rats in a CFA-induced inflammation model. In contrast with SNI, the absence of PAP-I had no detectable effect upon CFA-induced mechanical hyperalgesia (Fig. 4*J*; $F_{(1,125)} = 0.275$, $p = 0.6006$). This result suggests that PAP-I transported to the peripheral nerves is not crucial for the forma-

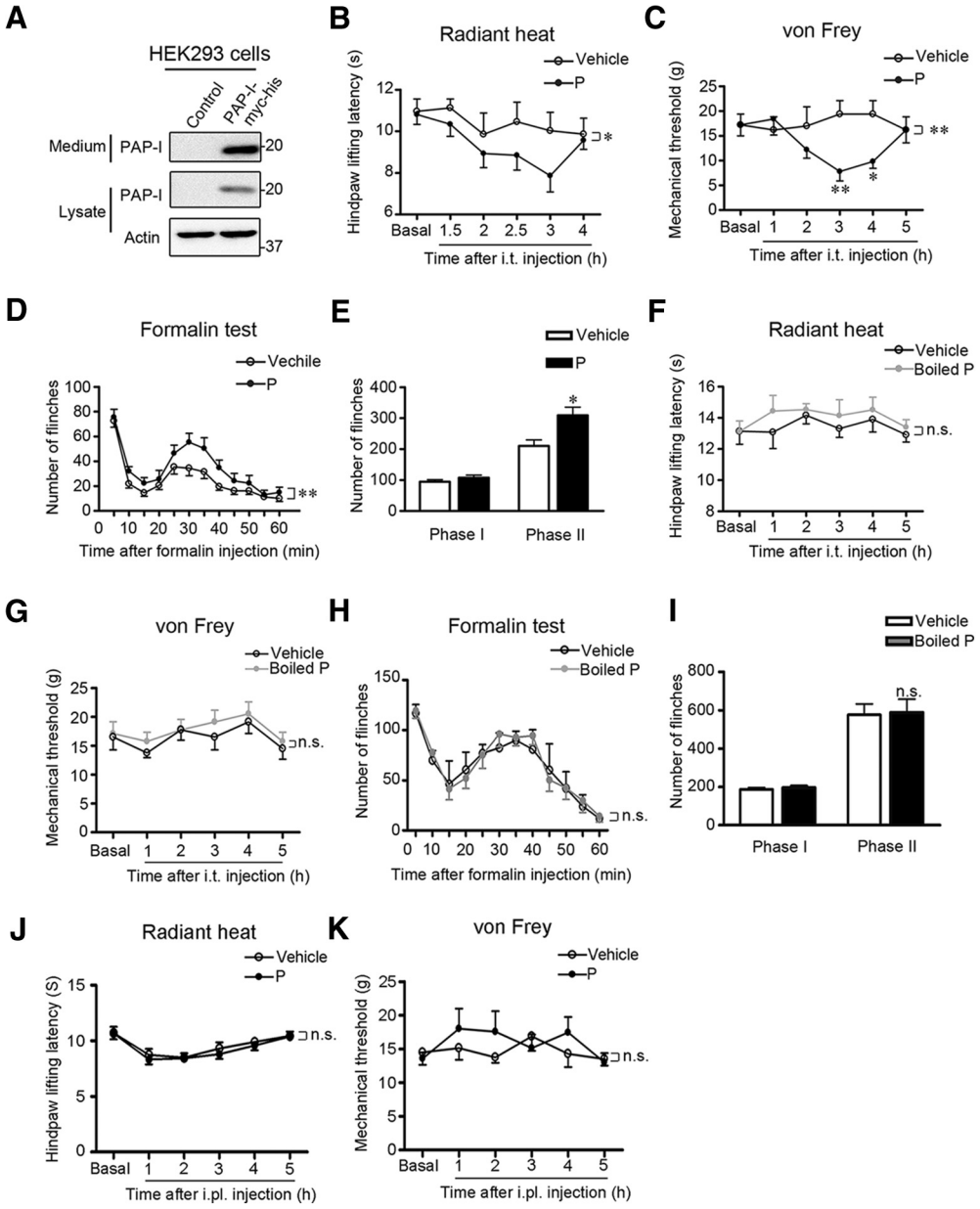

Figure 3. Central but not peripheral injection of PAP-I induces hyperalgesia. ***A***, Recombinant PAP-I-Myc-His was secreted by HEK293 cells into culture medium, from which it was concentrated and purified. ***B***, ***C***, Intrathecal (i.t.) injection of PAP-I-Myc-His (P, 2.5 μg/rat) induced a transient thermal (***B***, $n = 8$) and mechanical (***C***, $n = 6$) hyperalgesia in rats. The same amount of vehicle was used as control. ***D***, ***E***, PAP-I-Myc-His (2.5 μg/rat) was intrathecally injected into rats 30 min before intraplantar injection of 1% formalin. PAP-I-Myc-His promoted the nociceptive response, especially the Phase II (10–60 min) in formalin test ($n = 10$). ***F–I***, PAP-I-Myc-His was boiled at 100°C for 10 min to be denatured. Boiled PAP-I-Myc-His (Boiled P, 2.5 μg/rat) was intrathecally injected into normal Sprague Dawley rats for radiant heat test (***F***), von Frey test (***G***), and formalin test (***H***,***I***). The same amount of vehicle was used as control. In radiant heat test: $n = 6$ for boiled PAP-I-Myc-His and $n = 6$ for vehicle. In von Frey test: $n = 8$ for boiled PAP-I-Myc-His and $n = 8$ for vehicle. In formalin test: $n = 5$ for boiled PAP-I-Myc-His and $n = 3$ for vehicle. ***J***, Intraplantar (i.pl.) injection of 5 μg PAP-I-Myc-His ($n = 7$) did not affect thermal nociception in the radiant heat test. Vehicle was used as control ($n = 7$). ***K***, Intraplantar injection of PAP-I-Myc-His ($n = 7$) did not affect mechanical nociception in von Frey test. Vehicle was used as control ($n = 8$). Comparison between two curves (two-way ANOVA): $^*p < 0.05$; $^{**}p < 0.01$. $^*p < 0.05$ versus vehicle. $^{**}p < 0.01$ versus vehicle. n.s., not significant. Data are mean ± SEM.

tion of hypersensitivity, and further supports that PAP-I transported to the spinal cord participates in the maintenance of neuropathic pain.

PAP-I activates the spinal microglia

Previous studies report that some members of the PAP family are able to activate and attract peripheral macrophage (Namikawa et al., 2005; Viterbo et al., 2008; Lörchner et al., 2015). Considering the similarities between macrophage and microglia, we assumed microglia to be the potential target of PAP-I in the dorsal horn of spinal cord. To verify this hypothesis, we cultured primary microglia from rat spinal cord at P14, and stimulated the cells with PAP-I-Myc-His, while the endotoxin lipopolysaccharide (LPS)-induced inflammatory reaction was used as positive control. Immunostaining with F-actin and ED1, a microglial marker, showed that the cell bodies of microglia were expanded after 48 h treatment of 500 ng/ml PAP-I-Myc-His ($t = 4.442$, df = 3, $p = 0.0212$), which was comparable with that induced by 50 ng/ml LPS ($t = 9.006$, df = 3, $p = 0.0029$) (Fig. 5*A*,*B*), suggesting that microglia underwent a robust metamorphosis in response to the

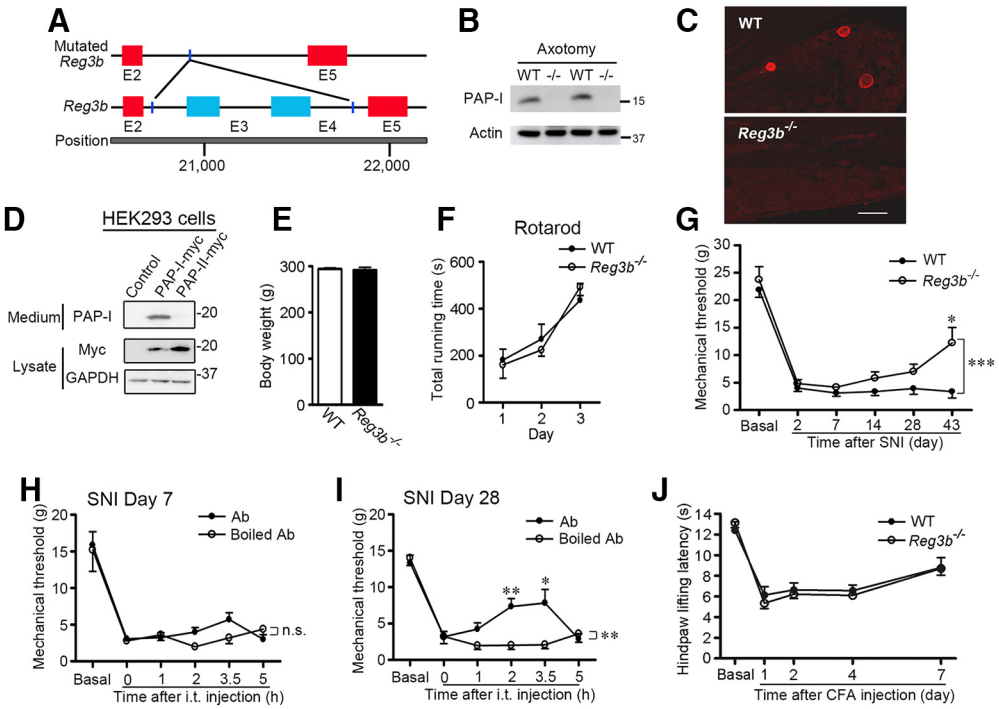

Figure 4. PAP-I is required for the formation of tactile allodynia after SNI. ***A***, Schematic diagram showing the construction of *Reg3b*$^{-/-}$ rat. A DNA segment, including exons 3 and 4 of *Reg3b* gene, was deleted using CRISPR/Cas9. ***B***, Immunoblotting showed the absence of PAP-I protein in the DRGs of *Reg3b*$^{-/-}$ rat (−/−), compared with WT littermates 7 d after axotomy of the sciatic nerve. ***C***, Immunostaining showed the absence of PAP-I protein in *Reg3b*$^{-/-}$ rat at SNI day 14. A WT littermate was used as positive control. Scale bar, 100 μm. ***D***, Immunoblotting showed the specificity of PAP-I antibody, which could not cross-react with PAP-II in HEK293 cells expressing PAP-II-myc-his. ***E***, The weight of adult *Reg3b*$^{-/-}$ rats ($n = 6$) and their WT littermates ($n = 5$). ***F***, Rotarod test of adult *Reg3b*$^{-/-}$ rats ($n = 8$) and their WT littermates ($n = 7$). ***G***, The tactile allodynia was gradually alleviated after SNI in *Reg3b*$^{-/-}$ rat ($n = 19$), compared with their WT littermates ($n = 16$). ***H***, ***I***, The effects of intrathecal (i.t.) injection of PAP-I antibody (Ab, 1 μg/rat) upon tactile allodynia after SNI. The antibody displayed no effect 7 d after SNI (***H***, $n = 7$) but significantly alleviated tactile allodynia 28 d after SNI (***I***, $n = 6$). Boiled antibody (Boiled Ab) was used as control ($n = 6$). ***J***, The CFA-induced thermal hyperalgesia was not affected in adult *Reg3b*$^{-/-}$ rats ($n = 16$), compared with their WT littermates ($n = 11$). Comparison between two curves (two-way ANOVA): $^{**}p < 0.01$; $^{***}p < 0.001$. $^{*}p < 0.05$ versus WT or boiled antibody. $^{**}p < 0.01$ versus WT or boiled antibody. n.s., not significant. Data are mean ± SEM.

PAP-I stimulation. Moreover, we used Boyden chamber (Fig. 5*C*) to test whether PAP-I had a chemotactic effect upon spinal microglia. The number of migrated microglia was increased markedly in the chamber containing 50 ng/ml ($t = 6.841$, df = 2, $p = 0.0207$) or 100 ng/ml ($t = 4.868$, df = 7, $p = 0.0018$) PAP-I-Myc-His (Fig. 5*D*,*E*). Thus, PAP-I directly activates spinal microglia.

To examine whether PAP-I directly sensitized DRG neurons, we did whole-cell patch-clamp recording on acutely dissociated DRG neurons. PAP-I-Myc-His was closely applied to one single neuron at a time to avoid the indirect effect of other cells (Fig. 5*F*). Whole-cell patch-clamp recording showed that the number of action potentials in response to the ramp stimulation was not increased after 30 min application of 500 ng/ml PAP-I-Myc-His to the DRG neurons from either naive rats or SNI rats (Fig. 5*G*,*H*). Interestingly, 500 ng/ml PAP-I-Myc-His even inhibited the activity of DRG neurons from SNI day 7 ($t = 2.300$, df = 22, $p = 0.0313$) rats (Fig. 5*G*,*H*). In addition, the drug delivering efficiency upon DRG neurons was similar between the perfusion system and direct incubation by comparing the neuronal activity induced by high potassium chloride (KCl) (Fig. 5*I*; $t = 1.243$, df = 16, $p = 0.2316$). These results exclude the possibility that PAP-I directly sensitizes DRG neurons after peripheral nerve injury.

The effect of PAP-I on microglia was then examined in the spinal dorsal horn. The status of spinal microglia was analyzed 3 h after intrathecal injection with 2.5 μg PAP-I-Myc-His. Immunostaining showed that both the total area ($t = 4.188$, df = 45, $p = 0.0001$) and intensity of Iba1 ($t = 4.722$, df = 45, $p < 0.0001$), a marker of spinal microglia, in the dorsal horn of L4–6 spinal cord, were distinctively increased, indicating a more active state of microglia (Fig. 6*A*,*B*). On the other hand, we immunostained the L4–6 spinal cord of *Reg3b*$^{-/-}$ rats at SNI day 43. The projection area of injured DRG neurons was marked by the disappearance of IB4 signal in the ipsilateral dorsal horn of spinal cord, and the border of lamina II was marked by protein kinase C gamma (Fig. 6*C*). Significantly, the total area and total intensity of Iba1 signal in the injured area of lamina I-II and III-V of ipsilateral dorsal horn were increased compared with those in the symmetrical area of the contralateral side in WT rats (Fig. 6*C–E*), indicating a robust microglial activation induced by nerve injury. Importantly, the activation of spinal microglia after SNI was impaired in *Reg3b*$^{-/-}$ rats (lamina I-II, Iba1 area ratio, $t = 5.825$, df = 12, $p < 0.0001$; Iba1 signal ratio, $t = 4.989$, df = 12, $p = 0.0003$; lamina III-V, Iba1 area ratio, $t = 2.365$, df = 12, $p = 0.0357$; Iba1 signal ratio, $t = 2.482$, df = 12, $p = 0.0289$) (Fig. 6*C–E*). These results suggest that PAP-I is necessary for microglial activation in the spinal dorsal horn after peripheral nerve injury.

Microglia activation is required for the pronociceptive effect of PAP-I

Based on above evidence showing an activation of spinal microglia by PAP-I, we tested whether the spinal microglia were the major target cells required for the pronociceptive effect of PAP-I. Minocycline, an inhibitor of microglia (Tikka et al., 2001; Hua et al., 2005), was intrathecally injected together with PAP-I-Myc-His to inhibit the activation of spinal microglia. Behavioral tests showed that intrathecal application of 50 μg minocycline almost

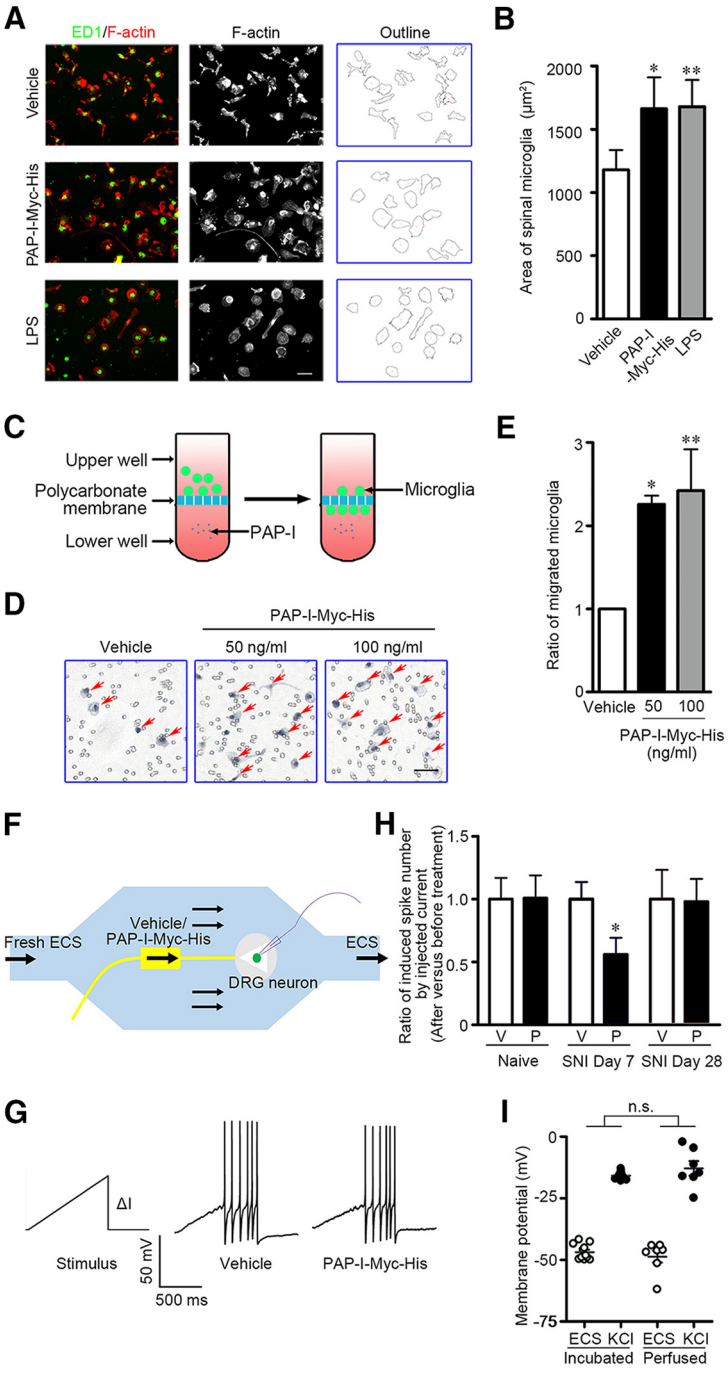

Figure 5. PAP-I activates cultured primary spinal microglia but not DRG neurons. ***A***, ***B***, PAP-I-Myc-His (500 ng/ml) induced the enlargement of cell area similar to LPS (50 ng/ml) in cultured primary spinal microglia. Primary spinal microglia were cultured with PAP-I-Myc-His (500 ng/ml) or LPS (50 ng/ml) for 48 h and then stained with ED1 (green) and phalloidin-labeled F-actin (red). The F-actin signal was used to outline the cells. Scale bar, 50 μm. The area of each cell was measured for quantitative analysis. ***B***, Data were from 4 independent experiments, and every group in each experiment includes 100–500 cells. ***C–E***, PAP-I-Myc-His caused chemotaxis of cultured primary spinal microglia in the Boyden chamber assay. ***C***, Schematic diagram shows the Boyden chamber structure and drug treatment. ***D***, The migrated microglia on the lower membrane were stained with hematoxylin. Red arrows indicate the migrated cells. Black circles represent membrane pores. Scale bar, 50 μm. The number of cells migrated under different concentrations of PAP-I-Myc-His were calculated and normalized to vehicle group (***E***, $n = 3$). ***F***, Schematic diagram showing the drug administration system used for whole-cell patch-clamp recording. ***G***, ***H***, Schematic diagram showing the ramp current stimulation (duration: 1 s, $\Delta I = 100$ pA for naive rats and $\Delta I = 150$ pA for SNI rats) and examples of membrane potential traces in response to the vehicle or 500 ng/ml PAP-I-Myc-His (***G***). ***H***, The number of induced spikes generated by PAP-I-Myc-His was not increased. In the naive group: $n = 10$ for vehicle (V) and $n = 12$ for PAP-I-Myc-His (P). In the SNI day 7 group: $n = 13$ for vehicle and $n = 11$ for PAP-I-Myc-His. In the SNI day 28 group: $n = 16$ for vehicle and $n = 14$ for PAP-I-Myc-His. ***I***, High K^+ solution (KCl) and extracellular solution (ECS) were either incubated with DRG neurons ($n = 11$) or applied to DRG neurons using the perfusion system ($n = 7$) to verify the efficiency of the perfusion system. *$p < 0.05$ versus vehicle. **$p < 0.01$ versus vehicle. n.s., not significant. Data are mean ± SEM.

completely blocked the thermal ($F_{(1,144)} = 5.604$, $p = 0.0193$) and mechanical hyperalgesia ($F_{(1,114)} = 11.480$, $p = 0.0010$; 2 h, $t = 2.625$, df = 20, $p = 0.0162$; 3 h, $t = 3.076$, df = 20, $p = 0.0060$) induced by 2.5 μg PAP-I-Myc-His (Fig. 7*A*,*B*). In the formalin test, intrathecal injection of 50 μg minocycline also completely blocked the enhancement of Phase II nociceptive response (Phase II, vehicle vs P, $t = 2.899$, df = 14, $p = 0.0117$; P vs P + Mino, $t = 3.392$, df = 13, $p = 0.0048$) induced by 2.5 μg PAP-I-Myc-His, making the level comparable with that of vehicle group (P vs P + Mino, $F_{(1,13)} = 14.730$, $p = 0.0021$; 25 min, $t = 4.508$, df = 13, $p = 0.0006$; 30 min, $t = 2.465$, df = 13, $p = 0.0284$; 35 min, $t = 2.336$, df = 13, $p = 0.0362$; 55 min, $t = 2.715$, df = 13, $p = 0.0177$) (Fig. 7*C*,*D*). Thus, PAP-I induces hyperalgesia mainly through activating microglia in the spinal cord.

CCR2-p38 MAPK pathway mediates the effect of PAP-I

Finally, we explored the molecular mechanism underlying the activation of spinal microglia by PAP-I. Secretory proteins usually display functions via affecting their interacting proteins on the cell membrane. Although two interacting proteins of PAP family have been reported, functional analysis is still needed to verify their interactions and identify downstream pathways (Kobayashi et al., 2000; Acquatella-Tran Van Ba et al., 2012). In the present study, a sequence-based machine learning method was adopted to predict the interacting membrane proteins with PAP-I. Among them, the 9 proteins in the top rank all belonged to chemokine receptor family (Fig. 8*A*). Although CCR6 had the highest score, its expression was low in spinal microglia and its relationship with pain was hardly reported (Hickman et al., 2013). On the other hand, CCR2 seemed more promising because previous studies reported that CCR2 was expressed in the spinal microglia and participated in chronic pain (Abbadie et al., 2003; Abbadie, 2005; Zhang et al., 2007).

Next, we used different approaches to verify the candidate. The single-cell PCR and immunoprecipitation from purified cultured primary microglia showed the expression of CCR2 mRNA and protein in microglia (Fig. 8*B*,*C*), which was consistent with previous microglia RNA-seq data (Hickman et al., 2013; Bennett et al., 2016). Coimmunoprecipitation experiments detected an interaction between PAP-I and CCR2 in the COS7 cells exogenously coexpressing PAP-I-HA and

Myc-CCR2, and in the rat pancreas-derived AR-42J cells endogenously expressing these two proteins (Fig. 8*D*,*E*). Previous study reported that p38 mitogen-activated protein kinase (p38 MAPK) was an important downstream pathway of CCR2 in the microglia activation (Abbadie et al., 2003). Consistently, immunoblotting showed that the phosphorylation level of p38 MAPK in cultured primary microglia was increased as soon as 30 min after 500 ng/ml PAP-I application (t = 18.500, df = 2, p = 0.0029) (Fig. 8*F*,*G*). Blocking this pathway using 200 nM VX-702 completely inhibited the morphological change (vehicle vs PAP-I, t = 2.900, df = 6, p = 0.0273; PAP-I vs VX-702, t = 3.651, df = 5, p = 0.0147) and chemotaxis (PAP-I vs VX-702, t = 3.890, df = 6, p = 0.0081) of spinal microglia induced by PAP-I-Myc-His (Fig. 8*H*,*I*). Similarly, application of 700 nM RS 504393, a CCR2 inhibitor, also completely blocked PAP-I-Myc-His-induced morphological change (PAP-I vs RS 504393, t = 3.875, df = 5, p = 0.0117) of spinal microglia (Fig. 8*H*,*I*). Therefore, the stimulating effect of PAP-I upon the spinal microglia could be mainly via the CCR2-p38 MAPK pathway.

Furthermore, we examined the role of CCR2 in PAP-I-induced hyperalgesia. First, we detected whether nerve injury altered the CCR2 expression in microglia. From isolated spinal microglia using FACS, quantitative PCR showed that the level of CCR2 mRNA was not remarkably changed in SNI day 7 rats (Fig. 8*J*; t = 2.150, df = 3, p = 0.1207). However, intrathecal injection of 25 μg RS 504393 completely blocked the thermal (P + DMSO vs P + RS 504393, $F_{(1,144)}$ = 26.250, $p < 0.0001$; 2 h, t = 2.770, df = 24, p = 0.0107; 3 h, t = 2.273, df = 24, p = 0.0323; 4 h, t = 3.741, df = 24, p = 0.0010) and mechanical hyperalgesia (P + DMSO vs P + RS 504393, $F_{(1,84)}$ = 10.330, p = 0.0019; 2 h, t = 2.995, df = 14, p = 0.0096; 3 h, t = 3.132, df = 14, p = 0.0074) induced by 2.5 μg PAP-I-Myc-His while having little effect upon rats injected with vehicle (Fig. 8*K*,*L*). In the formalin test, intrathecal injection of RS 504393 almost inhibited PAP-I-Myc-His-induced enhancement of Phase II nociceptive response (P + DMSO vs P + RS 504393, $F_{(1,14)}$ = 9.713, p = 0.0076; 30 min, t = 3.644, df = 14, p = 0.0027; 35 min, t = 3.516, df = 14, p = 0.0034; Phase II, V + DMSO vs P + DMSO, t = 2.314, df = 13, p = 0.0377; P + DMSO vs P + RS 504393, t = 3.289, df = 14, p = 0.0054) (Fig. 8*M*). Together, PAP-I activates the spinal microglia and induces hyperalgesia mainly via CCR2.

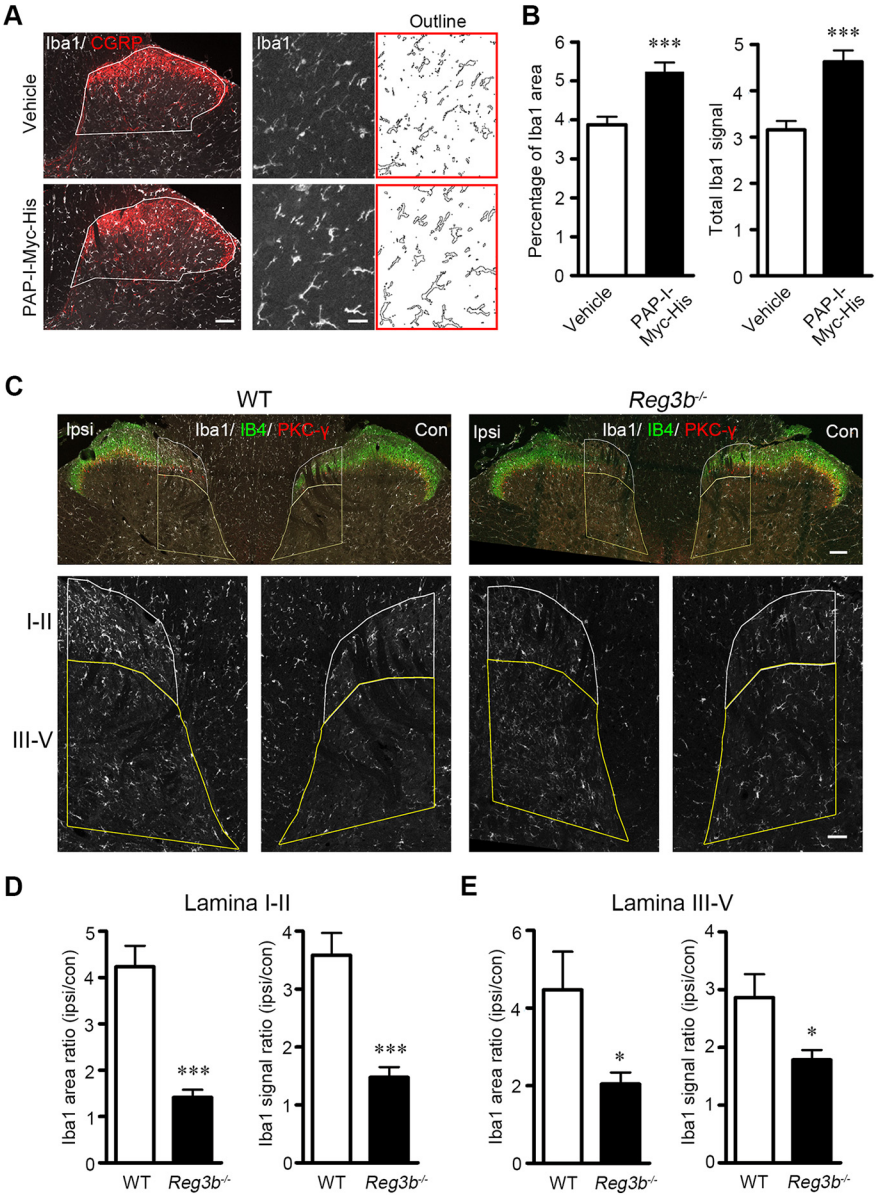

Figure 6. PAP-I is sufficient and necessary to activate microglia in the dorsal spinal cord. ***A***, ***B***, Intrathecal injection of PAP-I-Myc-His (2.5 μg/rat) induced morphological changes of spinal microglia. Microglia were labeled by Iba1 (white), and the afferent fibers were labeled by calcitonin-related polypeptide α (CGRP, red) in L4–6 spinal dorsal horn (***A***). Each dorsal horn was outlined for further analysis. Microglia were further magnified in spinal dorsal horn, and outlines of microglia were processed for subsequent quantitative analysis. Scale bars: entire spinal dorsal horn, 100 μm; magnified dorsal horn, 25 μm. In the area of spinal dorsal horn, the percentage of Iba1 area and total Iba1 signal was calculated (***B***). n = 4 for both PAP-I and vehicle groups. Three different dorsal spinal cord sections of each rat were used for quantification. ***C–E***, The activation of spinal microglia in the ipsilateral dorsal horn was alleviated in *Reg3b*$^{-/-}$ rats at SNI day 43. Microglia were labeled by Iba1 (white), and protein kinase C gamma (PKC-γ, red) marked the inner II of dorsal horn. Since the IB4 expression in DRG neurons was downregulated after SNI, the weakened IB4^{+} signal (green) in the central part of dorsal horn represented the region where the axons of injured DRG neurons terminated. The activation of spinal microglia was prominent in this area after SNI in rats. The central parts, including lamina I-II (white frame) and lamina III-V (yellow frame) of ipsilateral dorsal horn corresponding to the weakened IB4 signal, were outlined for further analysis. The same area of contralateral dorsal horn was used as control. Scale bars: top, 100 μm; bottom, 50 μm. In the selected dorsal horn area, the percentage of Iba1 signal area and average Iba1 signal intensity were calculated. Then, the ratio of ipsilateral versus contralateral dorsal horn was calculated to indicate the extent of spinal microglia activation in lamina I-II (***D***) and III-V (***E***). n = 4 for both WT and *Reg3b*$^{-/-}$ groups. *$p < 0.05$ versus vehicle or WT. ***$p < 0.001$ versus vehicle or WT. Data are mean ± SEM.

Discussion

The present study reveals the dynamic expression of PAP-I after SNI, and its function as a central proinflammatory factor, which contributes to the maintenance of neuropathic pain. Peripheral

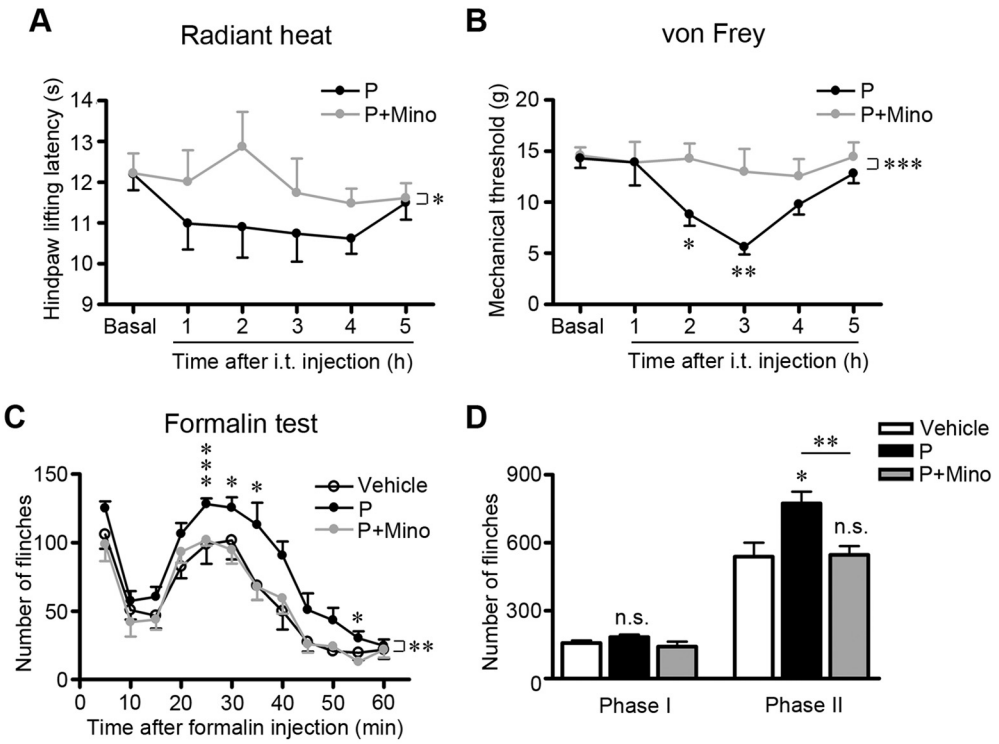

Figure 7. Inhibiting microglial activation blocks the pronociceptive effect of PAP-I in the spinal cord. ***A***, Intrathecal (i.t.) injection of the microglia inhibitor minocycline (50 μg/rat) blocked thermal hyperalgesia induced by PAP-I-Myc-His (2.5 μg/rat). $n = 13$ for PAP-I-Myc-His group (P) and $n = 13$ for inhibitor group (P + Mino). ***B***, Intrathecal (i.t.) injection of minocycline inhibited PAP-I-induced mechanical hyperalgesia. $n = 10$ for PAP-I-Myc-His group and $n = 11$ for inhibitor group. ***C***, ***D***, Intrathecal injection of minocycline inhibited PAP-I-induced enhancement of nociceptive response in formalin test. $n = 8$ for vehicle group, $n = 8$ for PAP-I-Myc-His group, and $n = 7$ for the inhibitor group. Comparison between two curves (P vs P + Mino, two-way ANOVA): $^*p < 0.05$; $^{**}p < 0.01$; $^{***}p < 0.001$. $^*p < 0.05$; $^{**}p < 0.01$; $^{***}p < 0.001$; versus P + Mino or vehicle. n.s., not significant. Data are mean ± SEM.

nerve injury triggers PAP-I expression in different types of DRG neurons in a time-dependent manner. The newly synthesized PAP-I can be transported to the spinal dorsal horn and activate the spinal microglia through the CCR2-p38 MAPK pathway. PAP-I does not affect the early establishment of SNI-induced tactile allodynia; however, its expression is very important for the long-term maintenance of tactile allodynia. Thus, the peripherally injured DRG neurons establish an immune crosstalk with the spinal microglia via PAP-I that leads to the long-term maintenance of neuropathic pain. This study may provide potential target for clinical neuropathic pain treatment.

PAP-I expression shifts among DRG neurons during the development of neuropathic pain

The present study showed that PAP-I was also *de novo* strongly expressed in DRG neurons after SNI. Interestingly, PAP-I was expressed in distinct types of DRG neurons during the progression of neuropathic pain. Similar size shift of PAP-I-expressing neurons occurred in the axotomy model (Averill et al., 2002) and even shared by PAP-II (He et al., 2010). The expression of other secretory neuropeptides, such as neuropeptide galanin, shifted between small and large DRG neurons after nerve injury (Villar et al., 1989; Xu et al., 2008). These dramatic changes may be due to the complicated mechanisms of neuropathic pain. The transition from normal sensation to allodynia consists of several processes: small DRG neurons that mainly mediates nociception are sensitized; some of the large neurons switch to participate in the transduction of nociception; microglia and astrocytes in the spinal cord are activated, changing circuit structure and connecting strength (Campbell and Meyer, 2006; Costigan et al., 2009). Thus, PAP-I expressed by different types of neurons at progressing states of neuropathic pain may have distinct functions in the functional aspects.

Another interesting finding is the different trafficking directions of PAP-I in SNI model and CFA-induced inflammation model. The ligation assay of dorsal roots and sciatic nerve proved that after CFA injection, most of PAP-I was transported along sciatic nerve to the periphery. However, in SNI model, PAP-I was accumulated not only in the sciatic nerve but also in the dorsal roots, suggesting a unique function of PAP-I in the spinal cord after nerve injury, which was confirmed by our behavior tests. It would be interesting to investigate the mechanisms underlying the directed trafficking of PAP-I in the sensory neurons.

PAP-I contributes to the maintenance of neuropathic pain

Behavior tests showed that PAP-I in the spinal cord could induce hyperalgesia. Notably, it was relatively slow for PAP-I to produce such an effect after intrathecal injection compared with several other molecules. Previous studies in our laboratory showed that secretory proteins, such as follistatin-like 1 (FSTL1), could induce the effects within minutes, reaching peak within 2 h (Li et al., 2011; Liu et al., 2012b). However, PAP-I took much longer time (3–4 h) to reach the maximum effect. The behavior test of PAP-I antibody injection at SNI day 28 was also consistent: the pain-relieving effect was most prominent around 3.5 h after injection. This slow effect of PAP-I may indeed support our hypothesis that PAP-I exerts its function by activating spinal microglia. FSTL1 acts quickly because it directly interacts with α1NKA on DRG neuronal membrane, and changes neuronal activity immediately (Li et al., 2011). On the other hand, PAP-I activates the spinal microglia, which may in turn sensitize the sensory circuit. This complex process would surely need more time to complete.

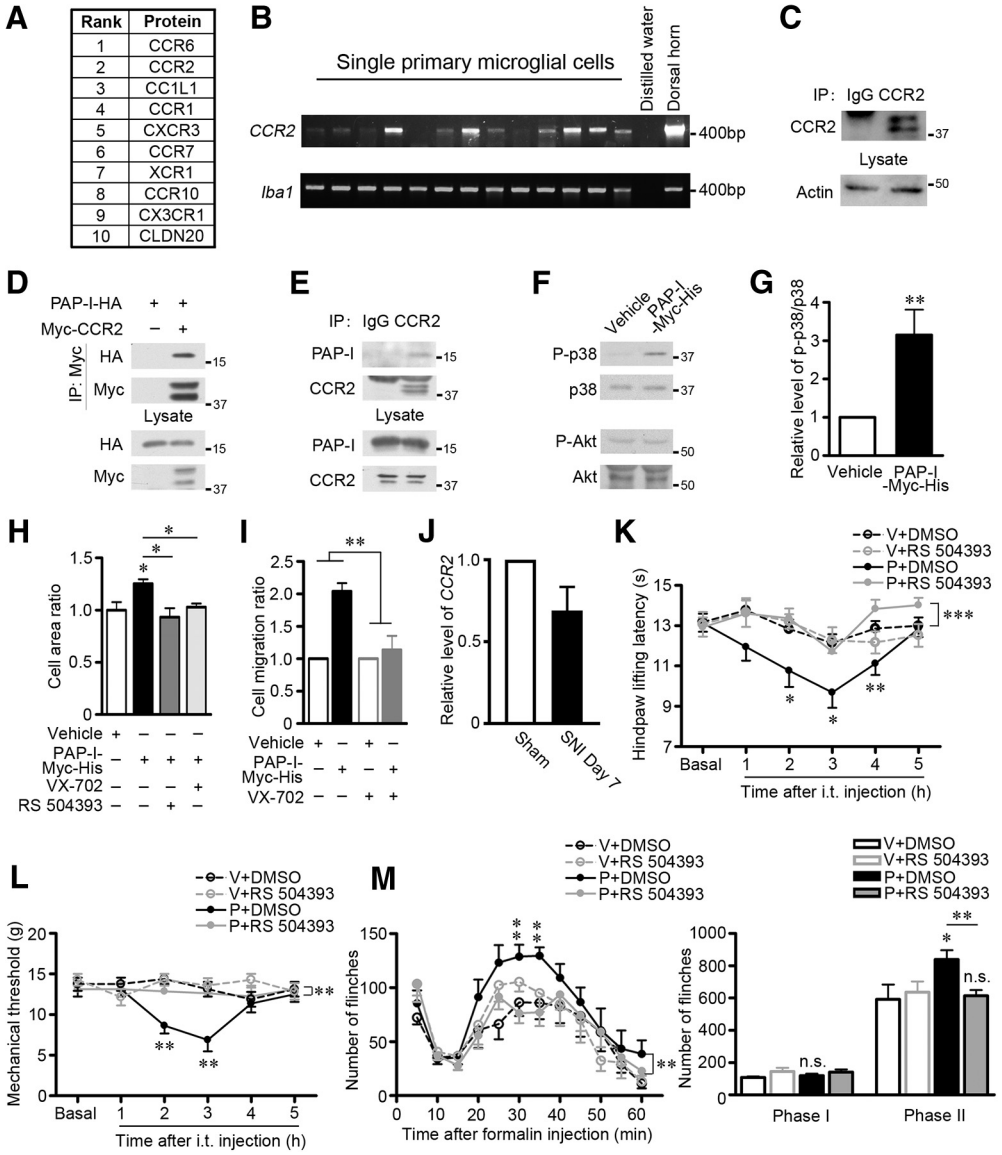

Figure 8. The CCR2–p38 MAPK pathway mediates the effect of PAP-I on the spinal microglia. ***A***, A computational prediction of the proteins that might interact with PAP-I. ***B***, The CCR2 mRNA was measured from single cultured primary microglia ($n = 13$). ***C***, Immunoblots showing CCR2 expression in cultured primary microglia. The CCR2 protein was enriched by immunoprecipitation (IP) with CCR2 antibody from protein extracts of cultured primary microglia. ***D***, ***E***, Immunoblots showing that PAP-I interacted with CCR2. Coimmunoprecipitation was performed with protein extracts from COS7 cells exogenously coexpressing PAP-I-HA and Myc-CCR2 using Myc antibody (***D***) or AR-42J cells endogenously expressing PAP-I and CCR2 using CCR2 antibody (***E***). ***F***, ***G***, Immunoblots showing that PAP-I-Myc-His induced an increased phosphorylation of p38 MAPK but not Akt in primary spinal microglia. Cultured microglia were treated with 500 ng/ml PAP-I-Myc-His for 30 min and then harvested for immunoblotting (***F***). Data were quantified and normalized to vehicle group (***G***, $n = 3$). ***H***, PAP-I-induced enlargement of microglia was blocked by p38 MAPK and CCR2 inhibitors. Primary spinal microglia were cultured with 500 ng/ml PAP-I-Myc-His, 200 nM VX-702, or 700 nM RS 504393 for 48 h and then stained with phalloidin-labeled F-actin to outline the cells. The area of each cell was measured for quantitative analysis (570, 792, 685, and 245 cells for vehicle, PAP-I-Myc-His, PAP-I-Myc-His + RS 504393, and PAP-I-Myc-His + VX-702 from 4 independent experiments, respectively). ***I***, Boyden chamber assay showing that the activation of p38 MAPK pathway was required for the chemotactic effect of PAP-I in primary spinal microglia. Both upper and lower wells were added with 200 nM VX-702. The migrated microglia on the lower side of membrane were stained with hematoxylin and counted. Data were normalized to vehicle or vehicle with VX-702 group ($n = 3$). ***J***, Quantitative PCR showed that the level of CCR2 mRNA in isolated spinal microglia was not significantly changed in SNI day 7 rats compared with sham group. $n = 4$. ***K***, Intrathecal (i.t.) injection of 25 μg RS 504393 together with 2.5 μg PAP-I-Myc-His did not induce thermal hyperalgesia in radiant heat test. $n = 21$ for vehicle (V) + DMSO group, $n = 10$ for V + RS 504393 group, $n = 13$ for PAP-I-Myc-His (P) + DMSO group, and $n = 13$ for P + RS 504393 group. ***L***, Intrathecal injection of RS 504393 together with PAP-I-Myc-His did not induce mechanical hyperalgesia in the von Frey test. $n = 7$ for V + RS 504393 group and $n = 8$ for each of the other three groups. ***M***, Intrathecal injection of RS 504393 together with PAP-I-Myc-His did not enhance the Phase II nociceptive response of formalin test. $n = 7$ for V + DMSO group, $n = 6$ for V + RS 504393 group, $n = 8$ for P + DMSO group, and $n = 8$ for P + RS 504393 group. Comparison between two curves (P + DMSO vs P + RS 504393) (two-way ANOVA): $^{**}p < 0.01$; $^{***}p < 0.001$. $^{*}p < 0.05$ versus vehicle or P + RS 504393 or indicated. $^{**}p < 0.01$ versus vehicle or P + RS 504393 or indicated. n.s., not significant. Data are mean ± SEM.

Most strikingly, although *Reg3b*$^{-/-}$ rats developed tactile allodynia like their littermates within 7 d after nerve injury, they failed to maintain it. At the initiating stage of neuropathic pain, DRG neurons upregulate a series of inflammatory factors (Campbell and Meyer, 2006; Costigan et al., 2009) to act upon neurons and glial cells. Many of them probably have stronger effect than PAP-I at early stage of neuropathic pain, thus compensating the effect of PAP-I deficiency. The mice lacking these molecules could not develop neuropathic pain. However, with the progression of neuropathic pain, these strong molecules, such as TNF-α, CXCL12, and MCP-1, are downregulated (Zhang and De Koninck, 2006; Bai et al., 2016); thus, the effect of PAP-I may

become more prominent. Consistently, neutralizing spinal PAP-I using a specific antibody at different time points after SNI led to different results. Blocking PAP-I at SNI day 7 had little effect; however, a lack of PAP-I at SNI day 28 quite significantly alleviated tactile allodynia. Interestingly, the pain-relieving effect by antibody blockade was more prominent than that in *Reg3b*$^{-/-}$ rats, which may be due to the compensating effect in chronic loss of PAP-I. Particularly, the reverse of tactile allodynia long after its establishment by blocking PAP-I highlights a potential target of PAP-I for neuropathic pain treatment.

The behavior results further verify and support each other to indicate that PAP-I mainly produces effects in the spinal cord rather than in the periphery. Intrathecal application of PAP-I induced strong pronociceptive effects, whereas peripheral delivery of PAP-I had no effect. Consistently, *Reg3b*$^{-/-}$ rats did not show alleviation of CFA-induced hyperalgesia; thus, endogenous PAP-I transported to the peripheral terminals of DRG neurons after CFA injection is not apparently involved in the formation of hypersensitivity.

In the case of SNI, PAP-I in the central terminals of DRG neurons is far more important than that in the periphery. However, circumstances may change in other cases. In diseases, such as acute pancreatitis and inflammatory bowel disease, PAP-I is upregulated and secreted in large quantity by visceral organs. Whether it could attract and activate the peripheral macrophage to sensitize sensory neurons innervating these organs and contribute to visceral pain is worthy to study. Moreover, spinal microglia are also reported to be activated through p38 MAPK pathway after pancreatitis and participate in pancreatitis-induced hyperalgesia (Liu et al., 2012a). Whether PAP-I is secreted into spinal dorsal horn by sensory neurons to activate microglia is also an interesting issue to study.

PAP-I activates the spinal microglia through the CCR2-p38 MAPK pathway

It is well known that the activation of spinal microglia plays an important role in the progression of neuropathic pain. The present study showed a marked reduction in the activation of spinal microglia in *Reg3b*$^{-/-}$ rats after SNI. More directly, cultured primary spinal microglia treated with PAP-I showed the shape change and chemotaxis, two indicators of microglial activation (Honda et al., 2001; Bianchi et al., 2011; Jeon et al., 2012). Moreover, intrathecal application of minocycline completely prevented the PAP-I-induced hyperalgesia. Therefore, the spinal microglia could be the major target for PAP-I secreted from the sensory afferents. On the other hand, although DRG neurons could also be affected by intrathecally injected substances, our whole-cell patch-clamp recording showed that PAP-I did not directly sensitize DRG neurons. These evidences support that PAP-I exerts a pronociceptive effect mainly through the spinal microglia.

Multiple signaling pathways mediate the activation of microglia during the formation of neuropathic pain. Our computational prediction combined with coimmunoprecipitation experiments indicate CCR2 to be the most promising interacting protein of PAP-I. It is accepted that the activation of microglial CCR2-p38 MAPK pathway is required for the progression of neuropathic pain (Abbadie et al., 2003; Abbadie, 2005; Ji and Suter, 2007). Consistently, inhibiting either CCR2 or p38 MAPK abolished the microglial activating effect induced by PAP-I. Although microglial activation is reported to be involved in the initiating phase of neuropathic pain (Marchand et al., 2005), our study revealed that in the SNI model, PAP-I participated in the activation of microglia at least 43 d after nerve injury, and was required for maintaining tactile allodynia. Various molecules activate the spinal microglia at different stages of neuropathic pain; nevertheless, PAP-I displayed this effect at the later stage. Therefore, PAP-I secreted from the afferent fibers activates a well-known immune response of the spinal microglia through the CCR2-p38 MAPK pathway, establishing a direct crosstalk between the injured peripheral sensory system and the central immune system.

Together, the present study reveals that PAP-I *de novo* expressed in DRG neurons after nerve injury acts as an endogenous proinflammatory factor mediating the crosstalk between the sensory neurons and spinal microglia. The role of PAP-I in maintaining the nerve injury-induced long-lasting tactile allodynia suggests that the blockade of the PAP-I/CCR2-p38 MAPK pathway could be a therapeutic target for the treatment of neuropathic pain.

References

Abbadie C (2005) Chemokines, chemokine receptors and pain. Trends Immunol 26:529–534.

Abbadie C, Lindia JA, Cumiskey AM, Peterson LB, Mudgett JS, Bayne EK, DeMartino JA, MacIntyre DE, Forrest MJ (2003) Impaired neuropathic pain responses in mice lacking the chemokine receptor CCR2. Proc Natl Acad Sci U S A 100:7947–7952.

Acquatella-Tran Van Ba I, Marchal S, François F, Silhol M, Lleres C, Michel B, Benyamin Y, Verdier JM, Trousse F, Marcilhac A (2012) Regenerating islet-derived 1alpha (Reg-1alpha) protein is new neuronal secreted factor that stimulates neurite outgrowth via exostosin tumor-like 3 (EXTL3) receptor. J Biol Chem 287:4726–4739.

Averill S, Davis DR, Shortland PJ, Priestley JV, Hunt SP (2002) Dynamic pattern of reg-2 expression in rat sensory neurons after peripheral nerve injury. J Neurosci 22:7493–7501.

Averill S, Inglis JJ, King VR, Thompson SW, Cafferty WB, Shortland PJ, Hunt SP, Kidd BL, Priestley JV (2008) Reg-2 expression in dorsal root ganglion neurons after adjuvant-induced monoarthritis. Neuroscience 155:1227–1236.

Bai L, Wang X, Li Z, Kong C, Zhao Y, Qian JL, Kan Q, Zhang W, Xu JT (2016) Upregulation of chemokine CXCL12 in the dorsal root ganglia and spinal cord contributes to the development and maintenance of neuropathic pain following spared nerve injury in rats. Neurosci Bull 32:27–40.

Bennett ML, Bennett FC, Liddelow SA, Ajami B, Zamanian JL, Fernhoff NB, Mulinyawe SB, Bohlen CJ, Adil A, Tucker A, Weissman IL, Chang EF, Li G, Grant GA, Hayden Gephart MG, Barres BA (2016) New tools for studying microglia in the mouse and human CNS. Proc Natl Acad Sci U S A 113:E1738–E1746.

Bianchi R, Kastrisianaki E, Giambanco I, Donato R (2011) S100B protein stimulates microglia migration via RAGE-dependent up-regulation of chemokine expression and release. J Biol Chem 286:7214–7226.

Bödeker H, Fiedler F, Keim V, Dagorn JC, Iovanna JL (1998) Pancreatitis-associated protein is upregulated in mouse pancreas during acute pancreatitis. Digestion 59:186–191.

Campbell JN, Meyer RA (2006) Mechanisms of neuropathic pain. Neuron 52:77–92.

Chen G, Zhang YQ, Qadri YJ, Serhan CN, Ji RR (2018) Microglia in pain: detrimental and protective roles in pathogenesis and resolution of pain. Neuron 100:1292–1311.

Costigan M, Befort K, Karchewski L, Griffin RS, D'Urso D, Allchorne A, Sitarski J, Mannion JW, Pratt RE, Woolf CJ (2002) Replicate high-density rat genome oligonucleotide microarrays reveal hundreds of regulated genes in the dorsal root ganglion after peripheral nerve injury. BMC Neurosci 3:16.

Costigan M, Scholz J, Woolf CJ (2009) Neuropathic pain: a maladaptive response of the nervous system to damage. Annu Rev Neurosci 32:1–32.

Decosterd I, Woolf CJ (2000) Spared nerve injury: an animal model of persistent peripheral neuropathic pain. Pain 87:149–158.

Dusetti NJ, Frigerio JM, Keim V, Dagorn JC, Iovanna JL (1993) Structural organization of the gene encoding the rat pancreatitis associated protein: analysis of its evolutionary history reveals an ancient divergence from the

other carbohydrate-recognition domain-containing genes. J Biol Chem 268:14470–14475.
Gironella M, Iovanna JL, Sans M, Gil F, Peñalva M, Closa D, Miquel R, Piqué JM, Panés J (2005) Anti-inflammatory effects of pancreatitis associated protein in inflammatory bowel disease. Gut 54:1244–1253.
Guan Z, Kuhn JA, Wang X, Colquitt B, Solorzano C, Vaman S, Guan AK, Evans-Reinsch Z, Braz J, Devor M, Abboud-Werner SL, Lanier LL, Lomvardas S, Basbaum AI (2016) Injured sensory neuron-derived CSF1 induces microglial proliferation and DAP12-dependent pain. Nat Neurosci 19:94–101.
Hammond TR, Dufort C, Dissing-Olesen L, Giera S, Young A, Wysoker A, Walker AJ, Gergits F, Segel M, Nemesh J, Marsh SE, Saunders A, Macosko E, Ginhoux F, Chen J, Franklin RJ, Piao X, McCarroll SA, Stevens B (2019) Single-cell RNA sequencing of microglia throughout the mouse lifespan and in the injured brain reveals complex cell-state changes. Immunity 50:253–271.e6.
He SQ, Yao JR, Zhang FX, Wang Q, Bao L, Zhang X (2010) Inflammation and nerve injury induce expression of pancreatitis-associated protein-II in primary sensory neurons. Mol Pain 6:23.
Hickman SE, Kingery ND, Ohsumi TK, Borowsky ML, Wang LC, Means TK, El Khoury J (2013) The microglial sensome revealed by direct RNA sequencing. Nat Neurosci 16:1896–1905.
Honda S, Sasaki Y, Ohsawa K, Imai Y, Nakamura Y, Inoue K, Kohsaka S (2001) Extracellular ATP or ADP induce chemotaxis of cultured microglia through Gi/o-coupled P2Y receptors. J Neurosci 21:1975–1982.
Hua XY, Svensson CI, Matsui T, Fitzsimmons B, Yaksh TL, Webb M (2005) Intrathecal minocycline attenuates peripheral inflammation-induced hyperalgesia by inhibiting p38 MAPK in spinal microglia. Eur J Neurosci 22:2431–2440.
Inoue K, Tsuda M (2018) Microglia in neuropathic pain: cellular and molecular mechanisms and therapeutic potential. Nat Rev Neurosci 19: 138–152.
Jeon H, Kim JH, Lee WH, Lee MS, Suk K (2012) Plasminogen activator inhibitor type 1 regulates microglial motility and phagocytic activity. J Neuroinflammation 9:149.
Ji RR, Suter MR (2007) p38 MAPK, microglial signaling, and neuropathic pain. Mol Pain 3:33.
Kettenmann H, Hanisch UK, Noda M, Verkhratsky A (2011) Physiology of microglia. Physiol Rev 91:461–553.
Kim D, You B, Jo EK, Han SK, Simon MI, Lee SJ (2010) NADPH oxidase 2-derived reactive oxygen species in spinal cord microglia contribute to peripheral nerve injury-induced neuropathic pain. Proc Natl Acad Sci U S A 107:14851–14856.
Kobayashi S, Akiyama T, Nata K, Abe M, Tajima M, Shervani NJ, Unno M, Matsuno S, Sasaki H, Takasawa S, Okamoto H (2000) Identification of a receptor for reg (regenerating gene) protein, a pancreatic beta-cell regeneration factor. J Biol Chem 275:10723–10726.
Kuner R (2010) Central mechanisms of pathological pain. Nat Med 16:1258–1266.
LaCroix-Fralish ML, Austin JS, Zheng FY, Levitin DJ, Mogil JS (2011) Patterns of pain: meta-analysis of microarray studies of pain. Pain 152: 1888–1898.
Li CL, Li KC, Wu D, Chen Y, Luo H, Zhao JR, Wang SS, Sun MM, Lu YJ, Zhong YQ, Hu XY, Hou R, Zhou BB, Bao L, Xiao HS, Zhang X (2016) Somatosensory neuron types identified by high-coverage single-cell RNA-sequencing and functional heterogeneity. Cell Res 26:967.
Li KC, Zhang FX, Li CL, Wang F, Yu MY, Zhong YQ, Zhang KH, Lu YJ, Wang Q, Ma XL, Yao JR, Wang JY, Lin LB, Han M, Zhang YQ, Kuner R, Xiao HS, Bao L, Gao X, Zhang X (2011) Follistatin-like 1 suppresses sensory afferent transmission by activating Na^+, K^+-ATPase. Neuron 69: 974–987.
Liu PY, Lu CL, Wang CC, Lee IH, Hsieh JC, Chen CC, Lee HF, Lin HC, Chang FY, Lee SD (2012a) Spinal microglia initiate and maintain hyperalgesia in a rat model of chronic pancreatitis. Gastroenterology 142:165–173.e2.
Liu XJ, Zhang FX, Liu H, Li KC, Lu YJ, Wu QF, Li JY, Wang B, Wang Q, Lin LB, Zhong YQ, Xiao HS, Bao L, Zhang X (2012b) Activin C expressed in nociceptive afferent neurons is required for suppressing inflammatory pain. Brain 135:391–403.
Liu ZP, Chen L (2012) Proteome-wide prediction of protein–protein interactions from high-throughput data. Protein Cell 3:508–520.
Livesey FJ, O'Brien JA, Li M, Smith AG, Murphy LJ, Hunt SP (1997) A Schwann cell mitogen accompanying regeneration of motor neurons. Nature 390:614–618.
Lörchner H, Pöling J, Gajawada P, Hou Y, Polyakova V, Kostin S, Adrian-Segarra JM, Boettger T, Wietelmann A, Warnecke H, Richter M, Kubin T, Braun T (2015) Myocardial healing requires Reg3β-dependent accumulation of macrophages in the ischemic heart. Nat Med 21:353–362.
Marchand F, Perretti M, McMahon SB (2005) Role of the immune system in chronic pain. Nat Rev Neurosci 6:521–532.
Mukherjee S, Zheng H, Derebe MG, Callenberg KM, Partch CL, Rollins D, Propheter DC, Rizo J, Grabe M, Jiang QX, Hooper LV (2014) Antibacterial membrane attack by a pore-forming intestinal C-type lectin. Nature 505:103–107.
Namikawa K, Fukushima M, Murakami K, Suzuki A, Takasawa S, Okamoto H, Kiyama H (2005) Expression of Reg/PAP family members during motor nerve regeneration in rat. Biochem Biophys Res Commun 332:126–134.
Nishimune H, Vasseur S, Wiese S, Birling MC, Holtmann B, Sendtner M, Iovanna JL, Henderson CE (2000) Reg-2 is a motoneuron neurotrophic factor and a signalling intermediate in the CNTF survival pathway. Nat Cell Biol 2:906–914.
Okubo M, Yamanaka H, Kobayashi K, Dai Y, Kanda H, Yagi H, Noguchi K (2016) Macrophage-colony stimulating factor derived from injured primary afferent induces proliferation of spinal microglia and neuropathic pain in rats. PLoS One 11:e0153375.
Prinz M, Priller J (2014) Microglia and brain macrophages in the molecular age: from origin to neuropsychiatric disease. Nat Rev Neurosci 15:300–312.
Shen J, Zhang J, Luo X, Zhu W, Yu K, Chen K, Li Y, Jiang H (2007) Predicting protein–protein interactions based only on sequences information. Proc Natl Acad Sci U S A 104:4337–4341.
Silva GA, Feeney C, Mills LR, Theriault E (1998) A novel and rapid method for culturing pure rat spinal cord astrocytes on untreated glass. J Neurosci Methods 80:75–79.
Thacker MA, Clark AK, Bishop T, Grist J, Yip PK, Moon LD, Thompson SW, Marchand F, McMahon SB (2009) CCL2 is a key mediator of microglia activation in neuropathic pain states. Eur J Pain 13:263–272.
Tikka T, Fiebich BL, Goldsteins G, Keinanen R, Koistinaho J (2001) Minocycline, a tetracycline derivative, is neuroprotective against excitotoxicity by inhibiting activation and proliferation of microglia. J Neurosci 21:2580–2588.
Tsuda M, Beggs S, Salter MW, Inoue K (2013) Microglia and intractable chronic pain. Glia 61:55–61.
Villar MJ, Cortés R, Theodorsson E, Wiesenfeld-Hallin Z, Schalling M, Fahrenkrug J, Emson PC, Hökfelt T (1989) Neuropeptide expression in rat dorsal root ganglion cells and spinal cord after peripheral nerve injury with special reference to galanin. Neuroscience 33:587–604.
Viterbo D, Bluth MH, Lin YY, Mueller CM, Wadgaonkar R, Zenilman ME (2008) Pancreatitis-associated protein 2 modulates inflammatory responses in macrophages. J Immunol 181:1948–1958.
Witting A, Möller T (2011) Microglia cell culture: a primer for the novice. Methods Mol Biol 758:49–66.
Xiao HS, Huang QH, Zhang FX, Bao L, Lu YJ, Guo C, Yang L, Huang WJ, Fu G, Xu SH, Cheng XP, Yan Q, Zhu ZD, Zhang X, Chen Z, Han ZG, Zhang X (2002) Identification of gene expression profile of dorsal root ganglion in the rat peripheral axotomy model of neuropathic pain. Proc Natl Acad Sci U S A 99:8360–8365.
Xu XJ, Hökfelt T, Wiesenfeld-Hallin Z (2008) Galanin and spinal pain mechanisms: where do we stand in 2008? Cell Mol Life Sci 65:1813–1819.
Zhang FX, Liu XJ, Gong LQ, Yao JR, Li KC, Li ZY, Lin LB, Lu YJ, Xiao HS, Bao L, Zhang XH, Zhang X (2010) Inhibition of inflammatory pain by activating B-type natriuretic peptide signal pathway in nociceptive sensory neurons. J Neurosci 30:10927–10938.
Zhang J, De Koninck Y (2006) Spatial and temporal relationship between monocyte chemoattractant protein-1 expression and spinal glial activation following peripheral nerve injury. J Neurochem 97:772–783.
Zhang J, Shi XQ, Echeverry S, Mogil JS, De Koninck Y, Rivest S (2007) Expression of CCR2 in both resident and bone marrow-derived microglia plays a critical role in neuropathic pain. J Neurosci 27:12396–12406.